Table 1. Summary of the Genetically Engineered Mice Involved in This Study

Mouse	Genotype	Phenotype
$COL7^{m-/-}$	Knockout mouse with targeted disruption of the mouse *Col7a1* encoding mouse type VII collagen	RDEB (severe disease phenotype)
$COL7^{m+/-}$	*Col7a1* heterozygous knockout mouse	Clinically normal
$COL7^{K14\text{-}h+}$	Transgenic mouse with human *COL7A1* driven by the human K14 promoter	Clinically normal
$COL7^{col1\text{-}h+}$	Transgenic mouse with human *COL7A1* driven by the promoter of the gene encoding mouse pro-α 2 chain of type I collagen	Clinically normal
$COL7^{CMV\text{-}h+}$	Transgenic mouse with human *COL7A1* driven by the ubiquitous CMV promoter	Clinically normal
$COL7^{m-/-,\ K14\text{-}h+}$	*Col7a1* knockout mouse rescued by human *COL7A1* with the human K14 promoter	Clinically normal
$COL7^{m-/-,\ col1\text{-}h+}$	*Col7a1* knockout mouse rescued by human *COL7A1* with the mouse pro-α 2 chain of type I collagen promoter	Clinically normal
$COL7^{m-/-,\ CMV\text{-}h+}$	*Col7a1* knockout mouse rescued by human *COL7A1* with the CMV promoter	Clinically normal
$COL7^{K14\text{-}\Delta h+}$	Transgenic mouse with mutated human type VII collagen with 7528delG mutation under the human K14 promoter	Clinically normal
$COL7^{m-/-,\ K14\text{-}\Delta h+}$	*Col7a1* knockout mouse with the mutated human type VII collagen with 7528delG	RDEB (moderate disease phenotype)

promoters were designated as K14Tg mice ($COL7^{K14\text{-}h+}$), col1a2Tg mice ($COL7^{col1\text{-}h+}$), and CMVTg mice ($COL7^{CMV\text{-}h+}$), respectively (Table 1).

Transgenic Rescue Experiment

Transgenic mice with different promoters ($COL7^{K14\text{-}h+}$, $COL7^{col1\text{-}h+}$, and $COL7^{CMV\text{-}h+}$) were crossbred to heterozygous *col7a1* knockout mouse ($COL7^{m+/-}$) generated by Heinonen et al[3] to create heterozygous mice carrying human *COL7A1* cDNA. Then these mice were mated again with $COL7^{m+/-}$ mice to obtain a mouse that harbored the human COL7 gene in a *col7a1* knockout background. The resulting transgenic rescue mice, each with either the K14, col1a2, or CMV promoter, were, respectively, designated as $COL7^{m-/-,\ K14\text{-}h+}$, $COL7^{m-/-,\ col1\text{-}h+}$, and $COL7^{m-/-,\ CMV\text{-}h+}$ (Table 1). The rescued mice ($COL7^{m-/-,\ K14\text{-}h+}$, $COL7^{m-/-,\ col1\text{-}h+}$, and $COL7^{m-/-,\ CMV\text{-}h+}$) were analyzed by histopathological, immunofluorescence, and immunoblot analyses as described below. Whole-skin samples from the rescued mice were used for the immunoblot analysis.

RT-PCR and Western Blot Analysis

Mouse skin was obtained from the back of each mouse and incubated with 10 mg/ml dispase for 8 hours at 4°C to separate the epidermis and dermis. The epidermal and dermal sheets were minced, and total RNA was extracted using an RNeasy RNA extraction kit (Qiagen, Hilden, Germany). The cDNA was synthesized with the SuperScript First-Strand Synthesis System for RT-PCR (Invitrogen, Grand Island, NY) and subjected to PCR, using specific primers (forward, 5′-CTCAGTGGATGTTGCCTTTA-3′; reverse, 5′-TAAGAACACAATGTCAGCGG-3′) and the following thermal cycling parameters: 94°C for 5 minutes, 94°C for 1 minute, and 56°C for 1 minute; followed by 35 cycles at 72°C for 1 minute and 72°C for 7 minutes.

For Western blot analysis, the epidermal and dermal sheets were mixed with a protease inhibitor cocktail (Sigma-Aldrich, St. Louis, MO), homogenized, and centrifuged at 15,000 × *g*. The supernatant of each sample was separated on a 5% polyacrylamide gel under reducing conditions. Immunoblotting analysis was performed by incubation with the LH7.2 monoclonal antibody (1:1000) for 18 hours at 4°C and then with secondary goat anti-mouse IgG antibodies conjugated with peroxidase (1:2000) for 1 hour at 37°C. The resultant complexes were processed using the Phototope HRP Western Blot Detection System (Cell Signaling Technology, Beverly, MA) according to the manufacturer's protocol.

Histopathological, Immunofluorescence, Ultrastructural, and Immunoelectron Microscopic Analyses

Mouse skin samples were fixed in 10% formalin neutral buffer solution for paraffin embedding or were immediately frozen in OCT compound and stored at −80°C. Paraffin-embedded sections were cut to 5 μm and stained with H&E solution. Alternatively, the LH7.2 monoclonal antibody against the NC-1 amino-terminal domain of COL7 (Chemicon, Temecula, CA) was used for immunofluorescence staining on frozen sections from tissue samples embedded in OCT compound. The bound antibodies were detected with fluorescein isothiocyanate-conjugated goat anti-mouse IgG antibody (Jackson ImmunoResearch Laboratories, Inc., West Grove, PA). Nuclear counterstaining with propidium iodide was performed in some immunofluorescence labeling experiments.

For electron microscopic examination, skin specimens were fixed in 5% glutaraldehyde, postfixed in 1% osmium tetroxide, and stained en block in uranyl acetate. They were dehydrated in a graded ethanol series and embedded in Araldite 6005. Ultrathin sections were cut and stained with uranyl acetate and lead citrate. The sections were examined with a transmission electron microscope (H-7100; Hitachi, Tokyo, Japan) at 75 kV. For semiquantitative morphometric analysis, the number of anchoring fibrils on electron micrographs was counted and the number of anchoring fibrils per unit length of lamina

densa was estimated as number of anchoring fibrils/1 μm of lamina densa. Minimal anchoring fibril features required for quantification were the presence of an arch structure of fibrils inserted into the dermis from the lamina densa. Twenty electron microscopic sections were examined for each mouse line. For immunoelectron microscopic analysis, skin samples were cryofixed with liquid propane cooled with nitrogen, cryosubstituted at −80°C, and low temperature-embedded at −60°C in Lowicryl K11M resin before undergoing UV polymerization. Ultrathin sections were cut to 90 nm thickness. The LH7.2 monoclonal antibody was used as the primary antibody, and then a goat anti-rabbit IgG 10-nm gold-conjugated secondary antibody was used (Amersham, Poole, UK). The sections were stained with uranyl acetate and lead citrate and examined with a transmission electron microscope.

Transgenic Rescue Experiment with the Human Mutated Gene

We generated a full-length human *COL7A1* cDNA containing the c.7528delG mutation and replaced the normal human *COL7A1* cDNA K14 promoter construct (Figure 1A) with the human mutated *COL7A1* cDNA (c.7528delG). The guanine at 7528 is at the end of the collagenous domain of COL7, and the mutation creates a premature stop codon at 18 bp downstream. The expressed protein is a truncated COL7 lacking the NC-2 domain at the C terminus. Using the same techniques as described above, we produced transgenic mice by microinjection, screening PCR, and germline transmission. The transgenic mice ($COL7^{K14\text{-}\Delta h+}$) were crossbred to heterozygous *col7a1* knockout mouse ($COL7^{m-/-}$). Then these mice ($COL7^{m+/-,\ K14\text{-}\Delta h+}$) were intercrossed to obtain a mouse that harbored the mutated human COL7 gene in a *col7a1* knockout background (Table 1). The rescued mice ($COL7^{m-/-,\ K14\text{-}\Delta h+}$) were analyzed by histopathological, immunofluorescence, and immunoblot analyses as described above.

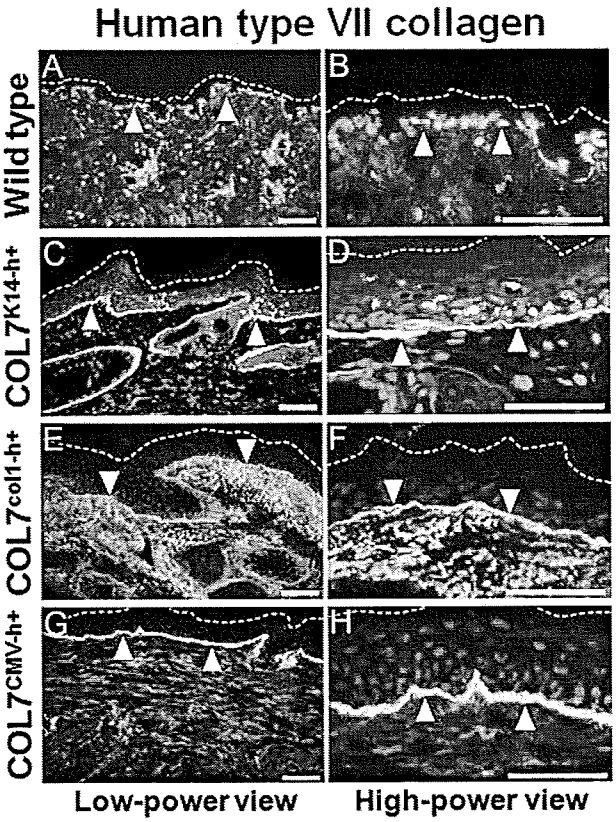

Figure 2. Both epidermis- and dermis-targeted transgene products of human COL7 molecules were precisely localized in the dermoepidermal junction in the transgenic mice. Immunofluorescence staining with the anti-human COL7 monoclonal antibody LH7.2 showed no human COL7 immunolabeling in the dermoepidermal junction of the wild-type mouse skin (**A** and **B**). Skin samples from all three transgenic mouse lines (keratinocyte-targeted K14Tg mice ($COL7^{K14\text{-}h+}$) (**C** and **D**), fibroblast-targeted col1a2Tg mice ($COL7^{col1\text{-}h+}$) (**E** and **F**), and CMVTg mice with ubiquitous COL7 expression ($COL7^{CMV\text{-}h+}$) (**G** and **H**) showed human COL7 linear staining at the epidermal BMZ (**white arrowheads**). $COL7^{K14\text{-}h+}$ mouse skin revealed additional punctate staining in epidermal keratinocytes, and $COL7^{col1\text{-}h+}$ mouse skin showed additional diffuse staining in dermal fibroblasts. Dotted lines demarcate the skin surface. Left column (**A, C, E,** and **G**), low-power view; right column (**B, D, F,** and **H**), high-power view. Human COL7 immunolabeling, green (fluorescein isothiocyanate); nuclear stain, red (propidium iodide). Scale bars = 50 μm.

Results

Generation of Transgenic Mice Showing Keratinocyte- or Fibroblast-Targeted Expression of Human COL7

To allow selective expression of human *COL7A1* in epidermal keratinocytes or in dermal fibroblasts, we used human K14 and mouse col1a2 promoters, which have been shown to specify epidermal and dermal expression in mice, respectively.[10,11] The mice with K14 or col1a2 promoters were designated as K14Tg mice ($COL7^{K14\text{-}h+}$) and col1a2Tg mice ($COL7^{col1\text{-}h+}$), respectively (Figure 1A). In addition, the ubiquitous CMV promoter was used to generate transgenic mice with both epidermal and dermal expression (CMVTg mice: $COL7^{CMV\text{-}h+}$) (Figure 1A). To demonstrate tissue-specific expression, we obtained epidermis and dermis from the mice and determined *COL7A1* mRNA expression by RT-PCR analysis using primers specific for human transcripts. The results show that $COL7^{K14\text{-}h+}$ mice *COL7A1* mRNA expression is restricted to the epidermis and mRNA expression of *COL7A1* in $COL7^{col1\text{-}h+}$ mice is restricted to the dermis. Expression of epidermal and dermal *COL7A1* mRNA was detected in $COL7^{CMV\text{-}h+}$ mice (Figure 1B). Western blot analysis also shows epidermal or dermal expression mostly consistent with the specific promoters, except for a weak COL7 band detected in the dermal component from $COL7^{K14\text{-}h+}$ mice (Figure 1C). A small amount of COL7 secreted by epidermal keratinocytes moves into the dermal side. The weak COL7 band in the dermal component from $COL7^{K14\text{-}h+}$ mice probably reflects the translocated COL7 peptides.

Immunofluorescence study using LH7.2 anti-human COL7 monoclonal antibody showed the linear epidermal

BMZ staining in all three transgenic mice lines (Figure 2, A and B, wild-type; Figure 2, C and D, $COL7^{K14\text{-}h+}$; Figure 2, E and F, $COL7^{col1\text{-}h+}$; and Figure 2, G and H, $COL7^{CMV\text{-}h+}$). $COL7^{K14\text{-}h+}$ revealed additional punctate staining in epidermal keratinocytes (Figure 2, C and D), and $COL7^{col1\text{-}h+}$ revealed additional diffuse staining in dermal fibroblasts (Figure 2, E and F). In the course of the transgenic mouse experiments, we obtained several lines of mice and were able to generate offspring in $COL7^{K14\text{-}h+}$, $COL7^{col1\text{-}h+}$, and $COL7^{CMV\text{-}h+}$ lineages. In each transgenic line, we selected the mouse with the most robust *COL7A1* expression for the subsequent rescue experiments.

Keratinocyte-/Fibroblast-Targeted Transgenic Rescue of COL7 Knockout Mice

Col7a1 knockout mice ($COL7^{m-/-}$) exhibit a severe, recessive DEB phenotype, and these mice die within a few days after birth. We initiated transgenic rescue experiments of $COL7^{m-/-}$ mice by mating $COL7^{m+/-}$, $COL7^{col1\text{-}h+}$, or $COL7^{CMV\text{-}h+}$ transgenic mice. After further crossing, transgenic mice on a *col7a1* knockout background ($COL7^{m-/-,\ K14\text{-}h+}$, $COL7^{m-/-,\ col1\text{-}h+}$, and $COL7^{m-/-,\ CMV\text{-}h+}$) were generated, and they showed expression of human COL7 under the different promoters. All three different rescued mice ($COL7^{m-/-,\ K14\text{-}h+}$,

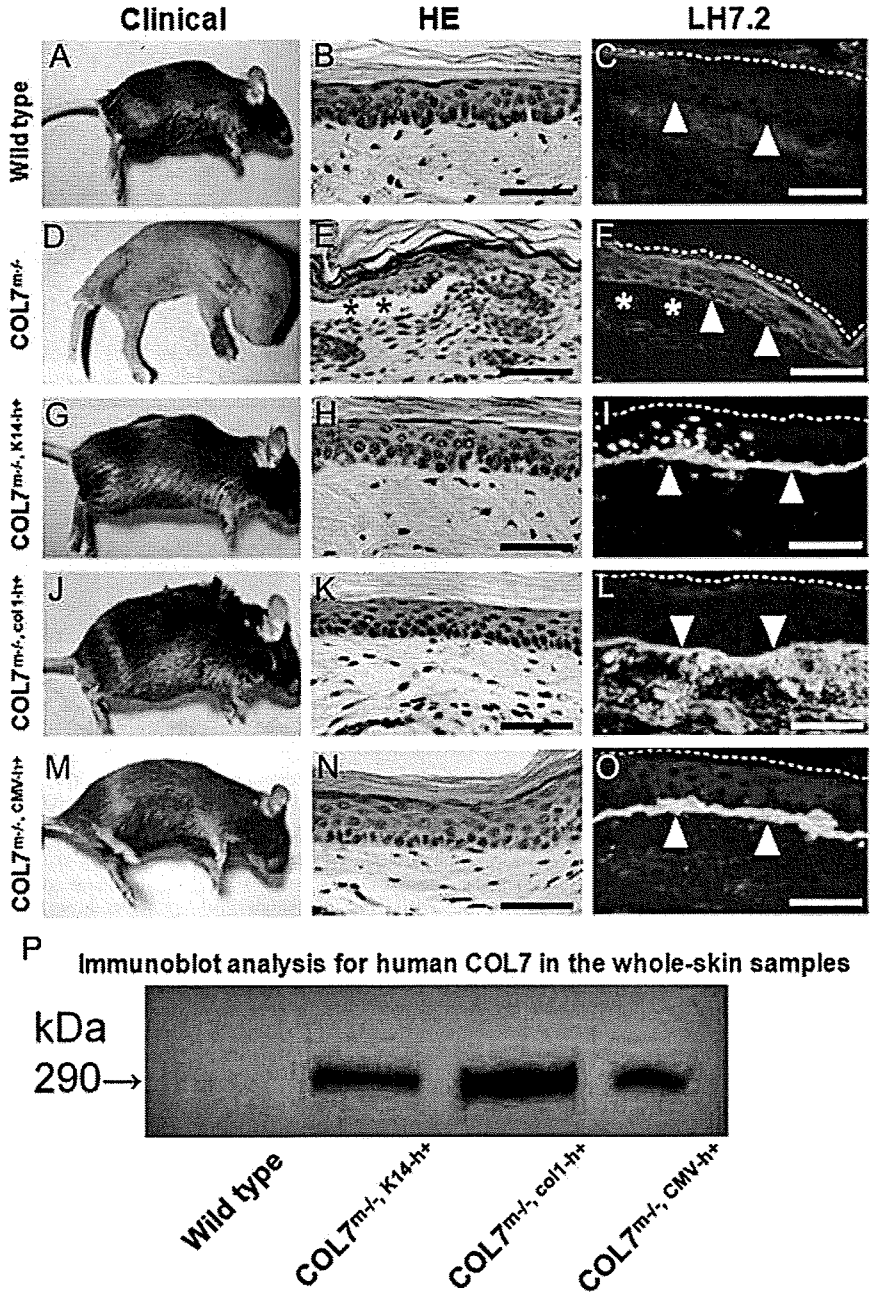

Figure 3. Keratinocyte-/fibroblast-targeted human *COL7A1* transgene can rescue COL7 knockout mice. A wild-type mouse showed a normal phenotype (**A**) and intact dermoepidermal junction (**B**) without human COL7 expression (**C, white arrowheads**). A $COL7^{m-/-}$ mouse had a severe DEB phenotype (**D**) and apparent dermoepidermal separation (**E, asterisks**) without human COL7 (**F, white arrowheads**). All three rescued mice (keratinocyte-targeted rescued $COL7^{m-/-,\ K14\text{-}h+}$ [**G–I**], fibroblast-targeted rescued $COL7^{m-/-,\ col1\text{-}h+}$ [**J–L**]), and ubiquitous CMV promoter-driven rescued $COL7^{m-/-,\ CMV\text{-}h+}$ [**M-O**]) showed no DEB phenotype (**G, J,** and **M**) and an intact dermoepidermal junction (**H, K,** and **N**). Immunofluorescence labeling revealed human COL7 in the basement membrane zone (**white arrowheads**) in skin sections from all three rescued mice (**I, L,** and **O**). Skin from the keratinocyte-targeted rescued $COL7^{m-/-,\ K14\text{-}h+}$ mouse showed additional punctate staining in epidermal keratinocytes (**I**), and skin from the fibroblast-targeted rescued $COL7^{m-/-,\ col1\text{-}h+}$ mouse revealed additional diffuse staining in dermal fibroblasts (**L**). Immunofluorescence staining with anti-human COL7 monoclonal antibody, LH7.2, fluorescein isothiocyanate, green (**C, F, I, L,** and **O**). **White arrowheads**, basement membrane zone; **asterisks,** a blister cavity. Dotted lines demarcate the skin surface. Scale bars = 50 μm. **P:** Immunoblot analysis for human COL7 in the whole-skin samples from the wild-type and the three rescued mouse lines. Human COL7 protein expression was confirmed in the whole skin of all three lines of rescued mice ($COL7^{m-/-,\ K14\text{-}h+}$, $COL7^{m-/-,\ col1\text{-}h+}$, and $COL7^{m-/-,\ CMV\text{-}h+}$) but not in the wild-type mice. From the density of immunoblot bands, amounts of human COL7 expressed in the whole-skin samples were the greatest in $COL7^{m-/-,\ col1\text{-}h+}$ line among the three lines of rescued mice. The other two rescued lines, $COL7^{m-/-,\ CMV\text{-}h+}$ and $COL7^{m-/-,\ K14\text{-}h+}$, expressed roughly similar amounts of human COL7.

COL7$^{m-/-,\ col1\text{-}h+}$, and COL7$^{m-/-,\ CMV\text{-}h+}$) showed normal appearance at birth, and no DEB phenotype was observed (Figure 3, A, D, G, J, and M). Remarkably, all of the rescued mice (COL7$^{m-/-,\ K14\ hours\text{-}+}$, COL7$^{m-/-,\ col1\text{-}h+}$, and COL7$^{m-/-,\ CMV\text{-}h+}$) exhibited reproductive ability despite the fact that the original COL7$^{m-/-}$ mice were lethal and unable to reproduce. All of these rescued mice had at least a 1-year lifespan, similar to that of wild-type mice. We could not detect any blistering, even on a histological scale (Figure 3, B, E, H, K, and N) and immunofluorescence study using LH7.2 showed positive linear staining of COL7 along the BMZ in all three lines of rescued mice (COL7$^{m-/-,\ K14\text{-}h+}$, COL7$^{m-/-,\ col1\text{-}h+}$, and COL7$^{m-/-,\ CMV\text{-}h+}$) (Figure 3, C, F, I, L, and O). The pattern of positive staining was essentially identical to that in the respective original transgenic mice (Figure 2, A–H). Immunoblot analysis for human COL7 in the whole-skin samples from the transgenic rescued mice confirmed that human COL7 protein was expressed in the whole skin of all three lines of rescued mice (COL7$^{m-/-,\ K14\text{-}h+}$, COL7$^{m-/-,\ col1\text{-}h+}$, and COL7$^{m-/-,\ CMV\text{-}h+}$) (Figure 3P). The thicknesses of the immunoblot bands suggested that, in the whole-skin samples, COL7$^{m-/-,\ col1\text{-}h+}$ expressed the most human COL7 among the three lines of rescued mice, and the other two rescued lines, COL7$^{m-/-,\ CMV\text{-}h+}$ and COL7$^{m-/-,\ K14\text{-}h+}$, produced similarly less human COL7.

Electron microscopy of the skin showed newly formed anchoring fibrils in the sublamina densa area in all of the rescued mice (COL7$^{m-/-,\ K14\text{-}h+}$, COL7$^{m-/-,\ col1\text{-}h+}$, and COL7$^{m-/-,\ CMV\text{-}h+}$) (Figure 4, A, C, E, G, and I). Semiquantitative morphometric analysis of numbers of anchoring fibrils on electron microscopic images revealed the anchoring fibril density in each mouse line as follows (mean ± SD number of anchoring fibrils/μm): wild-type COL7$^{m+/+}$, 3.41 ± 0.43; COL7$^{m-/-}$, 0.00 ± 0.00; COL7$^{m-/-,\ K14\text{-}h+}$, 2.60 ± 0.46; COL7$^{m-/-,\ col1\text{-}h+}$, 2.85 ± 0.39; and COL7$^{m-/-,\ CMV\text{-}h+}$, 3.09 ± 0.30 (Figure 4K). Immunoelectron microscopic analysis of the skin obtained from each line of rescued mice revealed that LH7.2-labeled gold particles were localized in the lamina densa of the BMZ (Figure 4, B, D, F, H, and J). The epitopes of LH7.2 monoclonal antibody are known to react to the NC-1 domain of COL7, which is known to be located along the lamina densa.[12] The results suggest that COL7 synthesized from transgenes functioned correctly, irrespective of whether it originated from fibroblasts or from keratinocytes.

Generation of an Exact DEB Model Mice Carrying Human COL7A1 Mutation

In the course of cloning experiments, we obtained several mutant *COL7A1* clones that demonstrated abnormal *COL7A1* expression. Subsequent sequence analysis revealed that one of those clones had a c.7528delG mutation in the *COL7A1* cDNA. We then constructed an expression vector of the mutated *COL7A1* under the K14 promoter and generated the transgenic mice. Next, we crossed these mutant COL7$^{K14\text{-}\Delta h+}$ transgenic mice with COL7$^{m+/-}$ het-

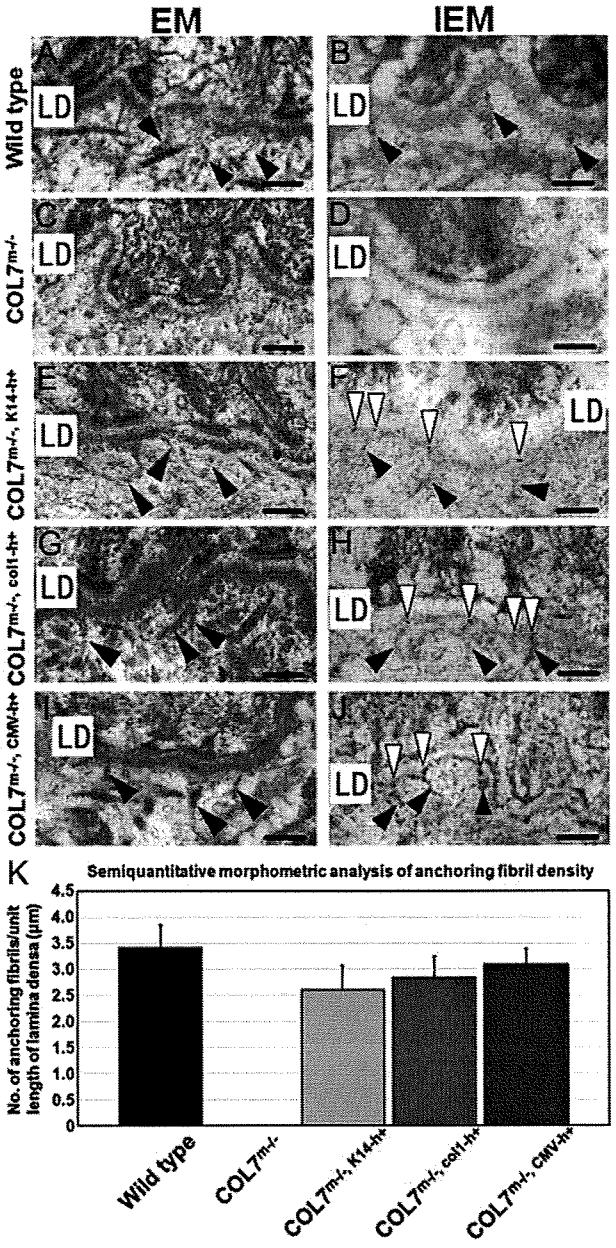

Figure 4. Transgene products, which are human COL7 molecules, correctly form anchoring fibrils in the rescued mice. Electron microscopy (EM) (**A, C, E, G,** and **I**) demonstrated intact anchoring fibrils (**black arrowheads**) in the sublamina densa area in a wild-type mouse (**A**). In contrast, the COL7$^{m-/-}$ mouse had no anchoring fibrils (**C**). In all three rescued mice lines (keratinocyte-targeted rescued COL7$^{m-/-,\ K14\text{-}h+}$ [**E**], fibroblast-targeted rescued COL7$^{m-/-,\ col1\text{-}h+}$ [**G**], and ubiquitous CMV promoter-driven rescued COL7$^{m-/-,\ CMV\text{-}h+}$ [**I**]), anchoring fibril formation was restored in the sublamina densa area (**black arrowheads**). Immunoelectron microscopy (IEM) using LH7.2 (**B, D, F, H,** and **J**) revealed no human COL7 labeling (gold particle) in intact anchoring fibrils (**black arrowheads**) of a wild-type mouse (**B**). The COL7$^{m-/-}$ mouse had neither anchoring fibrils nor human COL7 labeling (**D**). Human COL7 (immunogold particles, **white arrowheads**) was localized in the lamina densa of the basement membrane zone in all three rescued mice: keratinocyte-targeted rescued COL7$^{m-/-,\ K14\text{-}h+}$ (**F**), fibroblast-targeted rescued COL7$^{m-/-,\ col1\text{-}h+}$ (**H**), and ubiquitous CMV promoter-driven rescued COL7$^{m-/-,\ CMV\text{-}h+}$ (**J**). **Black arrowheads**, anchoring fibrils; **white arrowheads**, human COL7 labeling (immunogold particles); LD, lamina densa. Scale bars = 200 nm. **K:** Semiquantitative morphometric analysis of anchoring fibril density. Anchoring fibril density was highest in ubiquitous CMV promoter-driven rescued COL7$^{m-/-,\ CMV\text{-}h+}$, second highest in fibroblast-targeted rescued COL7$^{m-/-,\ col1\text{-}h+}$, and lowest in keratinocyte-targeted rescued COL7$^{m-/-,\ K14\text{-}h+}$ mice, among the three lines of rescued mice, although no statistically significant difference was observed between any combination of the three lines.

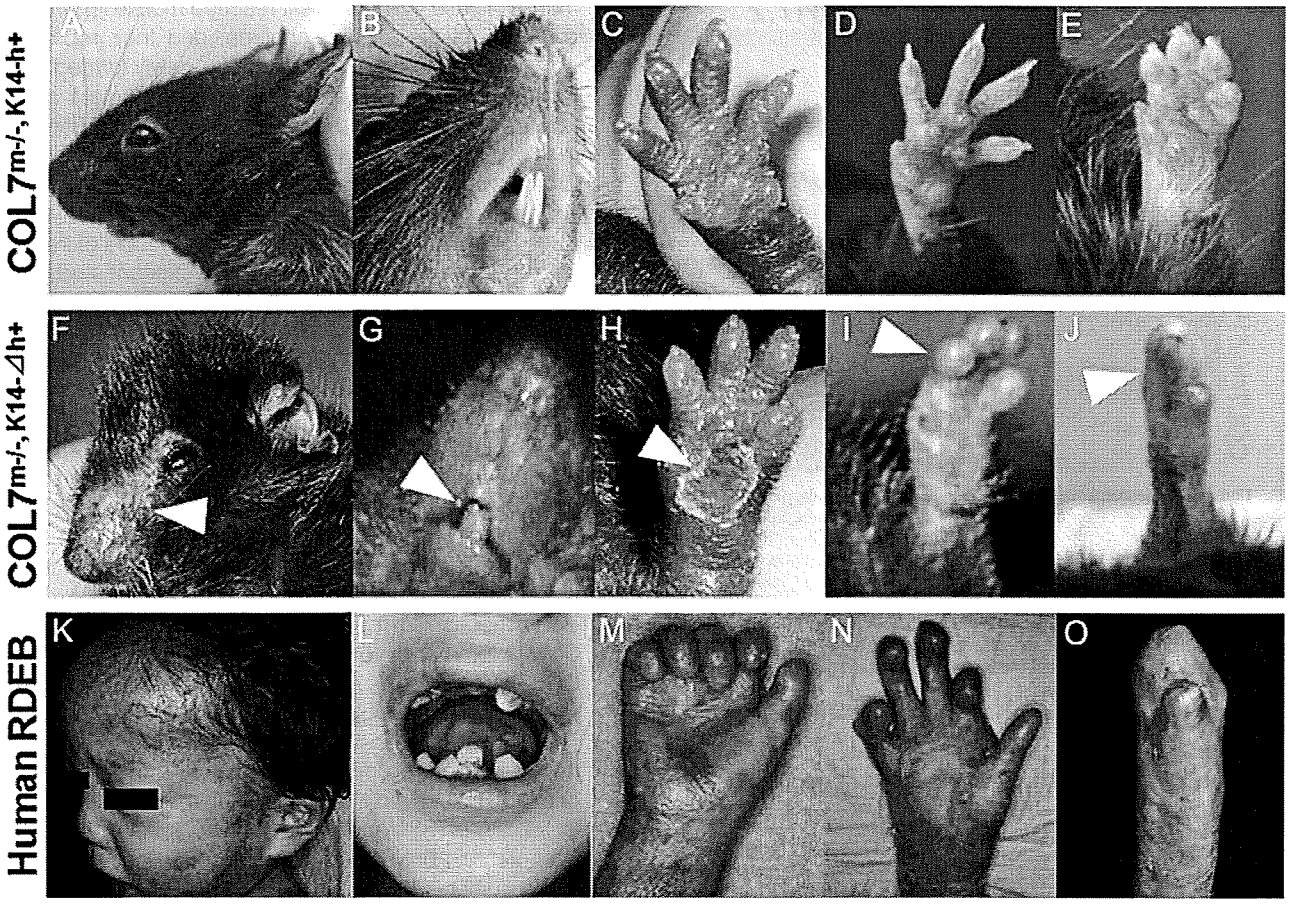

Figure 5. DEB model mice carrying a human *COL7A1* mutation precisely reproduce the DEB phenotype. **A–E:** *Col7a1* knockout mice rescued by full-length human *COL7A1* ($COL7^{m-/-, K14\text{-}h+}$) are clinically normal. Forepaws of $COL7^{m-/-, K14\text{-}h+}$ mice at 14 days (**C**), 30 days (**D**), and 60 days of age (**E**). **F–J:** *Col7a1* knockout mice rescued by mutated human *COL7A1* ($COL7^{m-/-, K14\text{-}\Delta h+}$) show gradual development of mild alopecia (**F**), yellowish dental caries (**G**), and fusion of the paw digits (**I** and **J**), corresponding to the clinical phenotype of human DEB. (**K** and **M:** A 2-year-old male patient harboring *COL7A1* mutations, c.[5818delC] + p.[Gly2623Ser].[13] **L:** A 10-year-old female patient whose mutations were unidentified. The diagnosis was confirmed by ultrastructural observation and immunofluorescence studies. **N:** A 15-year-old male patient with p.[Gly2576Arg] + [Glu2858X].[14] **O:** A 51-year-old female patient harboring p.[Gly1815Arg] + c.[5818delC].[15]) Forepaws of $COL7^{m-/-, K14\text{-}\Delta h+}$ mice were documented at 14 days (**H,** scarring), 30 days (**I,** mild fusion), and 60 days of age (**J,** complete fusion) (**white arrowheads**).

erozygous mice to obtain mutant $COL7^{m+/-, K14\text{-}\Delta h+}$ mice. We then performed transgenic rescue experiments by intercrossing these mice ($COL7^{m+/-, K14\text{-}\Delta h+}$) and obtained $COL7^{m-/-, K14\text{-}\Delta h+}$ mice. Immunoblot analysis on epidermal extract samples from $COL7^{m-/-, K14\text{-}\Delta h+}$ mice confirmed the expression of short, truncated human COL7 derived from mutant COL7A1 (data not shown).

From birth, the $COL7^{m-/-, K14\text{-}\Delta h+}$ mice were indistinguishable from their wild-type littermates and showed no blistering, not even on the paws, despite the fact that hemorrhagic bullae are always found in $COL7^{m-/-}$ mice. The growth of the human mutant-rescued mice ($COL7^{m-/-, K14\text{-}\Delta h+}$) was retarded, however, compared with that of their wild-type littermates. Interestingly, the $COL7^{m-/-, K14\text{-}\Delta h+}$ mice gradually developed the DEB phenotype, including nail dystrophy, scarring on the paws, fusion of the digits, yellowish dental caries, and mild alopecia, characteristic features of human RDEB (Figure 5, K–O).[13–15] It was difficult to distinguish the alopecia seen in the $COL7^{m-/-, K14\text{-}\Delta h+}$ mice from barbarism only from clinical appearance. However, the penetration of the alopecia is almost 100% in the $COL7^{m-/-, K14\text{-}\Delta h+}$ mice, whereas only a few wild-type littermates that were kept in the same condition showed barbarism. Thus, this alopecia was considered to be a feature specific to the $COL7^{m-/-, K14\text{-}\Delta h+}$ mice. These DEB clinical phenotypic manifestations were evident at 2 months of age (Figure 5, F–J). The clinical course of the forepaws showed a phenotype that is very characteristic of DEB. The $COL7^{m-/-, K14\text{-}\Delta h+}$ mice showed no blistering at birth, yet there was scarring of the forepaws 2 weeks later (Figure 5H). By 1 month, the paws had become mildly fused (Figure 5I), and complete fusion of paws (mitten deformity) was observed at 2 months (Figure 5J). The growth of the full-length human gene-rescued mice ($COL7^{m-/-, K14\text{-}h+}$) did not differ notably from that of the wild-type mice (Figure 5, A–E). During histopathological investigation, although clinically detectable blistering was not observed, we demonstrated microblistering along the dermal-epidermal junction in these mice ($COL7^{m-/-, K14\text{-}\Delta h+}$) by histopathological analysis (Figure 6, A and C). Immunofluorescence analysis showed immunoreactivity of human COL7 in the BMZ of the $COL7^{m-/-, K14\text{-}\Delta h+}$ mice (Figure 6, B and D). Most of the human mutant mice had about a 6-month lifespan (Figure 5,

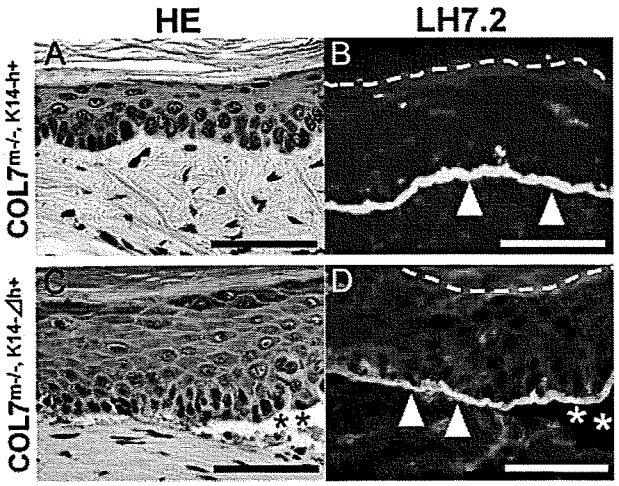

Figure 6. The humanized DEB model mouse shows subepidermal blistering with deposition of mutant human COL7 at the dermoepidermal junction. **A:** A $COL7^{m-/-,\ K14\text{-}h+}$ mouse has histopathologically normal skin. **C:** A $COL7^{m-/-,\ K14\text{-}\Delta h+}$ mouse shows subepidermal blistering (**asterisks**). **B** and **D:** Immunofluorescence study using anti-human COL7 antibody, LH7.2, reveals positive linear staining within the BMZ (**white arrowheads**), corresponding to normal and mutant human COL7 in a $COL7^{m-/-,\ K14\text{-}h+}$ mouse and a $COL7^{m-/-,\ K14\text{-}\Delta h+}$ mouse, respectively (**asterisks** indicate a blister cavity). Dotted lines demarcate the skin surface. Scale bars = 50 μm.

F-J). Thus, the clinical manifestations of human DEB were reproduced in the mouse by corrective transfer of human mutated *COL7A1* gene.

Discussion

COL7 is a major component of anchoring fibril loop structures beneath the epidermal basement membrane.[12,16] Previous studies have indicated that epidermal keratinocytes are the primary source of COL7 in developing human skin.[5,6] Thus, epidermal keratinocytes have been the main focus in the development of corrective gene therapies for DEB caused by *COL7A1* mutations. However, we recently showed that gene-transferred fibroblasts can supply a larger proportion of COL7 to the new dermal-epidermal junction as efficiently as gene-transferred keratinocytes.[17] Moreover, fibroblasts are more robust and less susceptible to growth arrest and differentiation than are epidermal keratinocytes.[6] Our study is are the first *in vivo* study to show that keratinocytes and fibroblasts, through direct comparative studies, are both feasible targets for DEB gene therapy. In addition, this study can be extended to other basement membrane proteins, and fibroblasts may provide those proteins from the dermis toward the epidermis.

We first generated several transgenic mice with COL7 expression under the control of each of the following promoters: K14, col1a2, and CMV. We have shown that COL7 expression from either keratinocytes or dermal fibroblasts can be fully integrated into the epidermal BMZ *in vivo*. We have also shown that expression of COL7 by either keratinocytes or fibroblasts can successfully rescue $COL7^{m-/-}$ mice.[3] Consequently, the rescued mice ($COL7^{m-/-,\ K14\text{-}h+}$, $COL7^{m-/-,\ col1\text{-}h+}$, and $COL7^{m-/-,\ CMV\text{-}h+}$) show expression of human COL7 under the control of the different promoters. These three different rescued mouse lines show no evidence of the DEB phenotype, and their reproductive ability was restored. Ultrastructurally, newly formed anchoring fibrils were present, and the NC-1 domain of COL7 localized precisely in the lamina densa of the BMZ in the rescued mice. Collectively, these results provide future prospects for corrective gene therapy for DEB.

Generally speaking, the nature of promoters used in transgenes does not always define the amount of transgene expression in transgenic mice. In the present study, immunofluorescence and immunoblot analysis suggested that fibroblast-targeted rescued $COL7^{m-/-,\ col1\text{-}h+}$ mice expressed more human COL7 than that expressed in ubiquitous CMV promoter-driven rescued $COL7^{m-/-,\ CMV\text{-}h+}$ mice and keratinocyte-targeted rescued $COL7^{m-/-,\ K14\text{-}h+}$ mice. Interestingly, in contrast, semiquantitative morphometric analysis of anchoring fibril density revealed that anchoring fibril density was highest in the ubiquitous CMV promoter-driven rescued $COL7^{m-/-,\ CMV\text{-}h+}$ mice, among the three lines of rescued mice, although no statistically significant difference was confirmed. We cannot explain the exact mechanism behind this discrepancy. In ubiquitous CMV promoter-driven rescued $COL7^{m-/-,\ CMV\text{-}h+}$ skin, COL7 is produced by both fibroblasts and keratinocytes, similar to the physiological manner of COL7 expression. Thus, we speculate that, in $COL7^{m-/-,\ CMV\text{-}h+}$ skin, COL7 peptides might be more efficiently assembled to form anchoring fibrils, even if less protein is expressed than in the $COL7^{m-/-,\ col1\text{-}h+}$ or $COL7^{m-/-,\ K14\text{-}h+}$ skin in which COL7 is expressed only by fibroblasts or keratinocytes, respectively.

The mice developed in this study can also provide a useful model for immunobullous diseases involving COL7. Recently, we succeeded in generating a bullous pemphigoid model.[18] Passive transfer of bullous pemphigoid autoantibodies into wild-type mice has failed to induce skin lesions, because of differences between humans and mice in the amino acid sequence of the pathogenic epitope of the autoantigen, COL7.[19] We injected the patients' autoantibody into murine COL7 knockout mice that had been rescued by the expression of the human autoantigen. This resulted in successful reactions by autoantigens and autoantibodies, thereby producing the bullous pemphigoid phenotype. Epidermolysis bullosa acquisita is an autoimmune blistering disorder, and the patients' autoantibodies react to COL7. Therefore, the rescued mice with humanized COL7 that we produced should be useful in future research on epidermolysis bullosa acquisita as well.

Another interesting aspect of the present study is that we were able to develop $COL7^{K14\text{-}\Delta h+}$ transgenic mice with human *COL7A1* cDNA containing the mutation c.7528delG. The $COL7^{K14\text{-}\Delta h+}$ transgenic mice and the $COL7^{m-/-,\ K14\text{-}\Delta h+}$ rescued mice showed positive human COL7 staining at the BMZ, indicating that COL7 without the NC-2 domain can still form a triple helix and be secreted by keratinocytes. The characteristic component of all collagens is the triple helix formed by three subunits, and its assembly is based on the repetition of the Gly-X-Y repeats. It has been suggested that a zipper-like mechanism of triple helix formation starts from the C

terminus toward the N terminus in collagens I and IV[20–22] and from the N-terminal to the C-terminal direction in epidermal type XVII collagen.[23] Our experiments using the genetically engineered mouse model suggest that the N- to C-terminal mechanism of triple helix formation is also possible for COL7. However, lack of the NC-2 domain, which is critical for antiparallel-dimer formation, might cause partial and weak immunoreactivity of human COL7 in the BMZ of COL7$^{m-/-, K14\text{-}\Delta h+/+}$ mice. This study demonstrates the importance of the NC-2 domain in COL7 formation and assembly *in vivo*.

Of importance, we have generated a mouse model of DEB that allows for long-term studies that were not possible with the previously generated neonatal lethal COL7$^{m-/-}$ *col7a1* knockout mice. A surviving DEB mouse model (the mouse COL7 hypomorphic mouse) that was recently reported expresses mouse COL7 at approximately 10% of normal levels.[4] These mice could survive longer than *Col7a1* knockout mouse (COL7$^{m-/-}$) and present clinical phenotypes (mitten hands and feet) similar to those of human DEB. The phenotypes of these model mice were produced from the gene-engineered mouse COL7 gene using a hypomorphic technique. These mice had a high mortality rate (67%) within 28 days without a change to a liquid diet consisting of infant milk. On the contrary, our novel mouse models of RDEB were generated by completely different methodology using a mutated human *COL7A1* gene, and the mouse could survive longer without use of a liquid diet. Surprisingly, our original DEB model mouse is very similar to humans not only in terms of clinical manifestations but also in terms of the genetic background. In fact, the COL7$^{m-/-, K14\text{-}\Delta h+}$ mice demonstrated nail dystrophy, scarring on the paws, fusion of the digits, yellowish dental caries, and mild alopecia, even in the absence of overt blistering. The previous *col7a1* knockout COL7$^{m-/-}$ mice developed spontaneous blistering soon after birth and died within several days.[3] Thus, COL7$^{m-/-}$ mice have not been available for long-term experiments. In this study, the production of rescued mice with mutated *COL7A1* (COL7$^{m-/-, K14\text{-}\Delta h+}$) has given us a surviving model of DEB. This model has great potential for future research into the pathomechanisms of DEB, wound healing, the development of squamous cell carcinomas, and the development of molecular therapies for patients with DEB.

Although we used cDNA with the mutation c.7528delG, which causes a premature stop termination codon (PTC), the consequences of the PTC mutation in the *COL7A1* cDNA are different from those in the *COL7A1* gene. Genomic PTC mutations are subject to nonsense-mediated mRNA decay, resulting in mRNA degradation in some instances. In the literature, genomic PTC mutations in *COL7A1* were previously reported to result in nonsense-mediated mRNA decay and absence of COL7 protein synthesis in severe generalized cases of RDEB.[24,25] Whether a genomic PTC mutation leads to nonsense-mediated mRNA decay depends on the mutation site.[26] In contrast, the PTC mutation in cDNA does not lead to mRNA decay and is thought to generate a truncated protein. In fact, we confirmed the expression of human COL7 derived from human mutant *COL7A1* in the COL7$^{m-/-, K14\text{-}\Delta h+}$ mice by immunoblot analysis (data not shown) and immunofluorescence staining (Figure 6D) in the present study. Approximately 300 distinct *COL7A1* mutations have been identified in patients with DEB around the world, and the clinical features, severity, prognosis, and response to treatment vary depending on the specific mutation.[15,24,27–31] Our understanding of how specific mutations produce differing clinical presentations and prognoses is limited. We believe that our systems have the advantage of being able to use human genes. Because the COL7 gene is almost 30 kb in size, introduction of the gene with PTC mutation might be impractical. However, if we generate the same mouse models with the patient-specific missense mutations in the cDNA or with the patient-specific PTC mutation in partial genomic DNA, which was inserted in the cDNA, then they might be useful for evaluating the prognosis of each patient with a certain mutation and for developing a mutation-specific treatment. This strategy could be extended to the development of therapies tailored to other, currently intractable inherited diseases.

Acknowledgments

We thank Ms. Akari Nagasaki and Ms. Shizuka Miyakoshi for their technical assistance.

References

1. Fine JD, Eady RA, Bauer EA, Bauer JW, Bruckner-Tuderman L, Heagerty A, Hintner H, Hovnanian A, Jonkman MF, Leigh I, McGrath JA, Mellerio JE, Murrell DF, Shimizu H, Uitto J, Vahlquist A, Woodley D, Zambruno G: The classification of inherited epidermolysis bullosa (EB): Report of the Third International Consensus Meeting on Diagnosis and Classification of EB. J Am Acad Dermatol 2008, 58:931–950
2. Uitto J, Pulkkinen L: Molecular genetics of heritable blistering disorders. Arch Dermatol 2001, 137:1458–1461
3. Heinonen S, Männikkö M, Klement JF, Whitaker-Menezes D, Murphy GF, Uitto J: Targeted inactivation of the type VII collagen gene (Col7a1) in mice results in severe blistering phenotype: a model for recessive dystrophic epidermolysis bullosa. J Cell Sci 1999, 112:3641–3648
4. Fritsch A, Loeckermann S, Kern JS, Braun A, Bösl MR, Bley TA, Schumann H, von Elverfeldt D, Paul D, Erlacher M, von Rautenfeld DB, Hausser I, Fässler R, Bruckner-Tuderman L: A hypomorphic mouse model of dystrophic epidermolysis bullosa reveals mechanisms of disease and response to fibroblast therapy. J Clin Invest 2008, 118:1669–1679
5. Ryynänen J, Sollberg S, Parente MG, Chung LC, Christiano AM, Uitto J: Type VII collagen gene expression by cultured human cells and in fetal skin: abundant mRNA and protein levels in epidermal keratinocytes. J Clin Invest 1992, 89:163–168
6. Goto M, Sawamura D, Ito K, Abe M, Nishie W, Sakai K, Shibaki A, Akiyama M, Shimizu H: Fibroblasts show more potential as target cells than keratinocytes in COL7A1 gene therapy of dystrophic epidermolysis bullosa. J Invest Dermatol 2006, 126:766–772
7. Ortiz-Urda S, Lin Q, Green CL, Keene DR, Marinkovich MP, Khavari PA: Injection of genetically engineered fibroblasts corrects regenerated human epidermolysis bullosa skin tissue. J Clin Invest 2003, 111:251–255
8. Woodley DT, Krueger GG, Jorgensen CM, Fairley JA, Atha T, Huang Y, Chan L, Keene DR, Chen M: Normal and gene-corrected dystrophic epidermolysis bullosa fibroblasts alone can produce type VII collagen at the basement membrane zone. J Invest Dermatol 2003, 121:1021–1028
9. Wong T, Gammon L, Liu L, Mellerio JE, Dopping-Hepenstal PJ, Pacy J, Elia G, Jeffery R, Leigh IM, Navsaria H, McGrath JA: Potential of

fibroblast cell therapy for recessive dystrophic epidermolysis bullosa. J Invest Dermatol 2008, 128:2179–2189
10. Shibaki A, Sato A, Vogel JC, Miyagawa F, Katz SI: Induction of GVHD-like skin disease by passively transferred $CD8^+$ T-cell receptor transgenic T cells into keratin 14-ovalbumin transgenic mice. J Invest Dermatol 2004, 123:109–115
11. Denton CP, Zheng B, Shiwen X, Zhang Z, Bou-Gharios G, Eberspaecher H, Black CM, de Crombrugghe B: Activation of a fibroblast-specific enhancer of the proalpha2(I) collagen gene in tight-skin mice. Arthritis Rheum 2001, 44:712–722
12. Shimizu H, Ishiko A, Masunaga T, Kurihara Y, Sato M, Bruckner-Tuderman L, Nishikawa T: Most anchoring fibrils in human skin originate and terminate in the lamina densa. Lab Invest 1997, 76:753–763
13. Sawamura D, Mochitomi Y, Kanzaki T, Nakamura H, Shimizu H: Glycine substitution mutations by different amino acids at the same codon in *COL7A1* cause different modes of dystrophic epidermolysis bullosa inheritance. Br J Dermatol 2006, 155:834–837
14. Shimizu H, McGrath JA, Christiano AM, Nishikawa T, Uitto J: Molecular basis of recessive dystrophic epidermolysis bullosa: genotype/phenotype correlation in a case of moderate clinical severity. J Invest Dermatol 1996, 106:119–124
15. Sawamura D, Goto M, Yasukawa K, Sato-Matsumura K, Nakamura H, Ito K, Nakamura H, Tomita Y, Shimizu H: Genetic studies of 20 Japanese families of dystrophic epidermolysis bullosa. J Hum Genet 2005, 50:543–546; erratum in J Hum Genet 2006, 51:839)
16. Uitto J, Chung-Honet LC, Christiano AM: Molecular biology and pathology of type VII collagen. Exp Dermatol 1992, 1:2–11
17. Woodley DT, Keene DR, Atha T, Huang Y, Ram R, Kasahara N, Chen M: Intradermal injection of lentiviral vectors corrects regenerated human dystrophic epidermolysis bullosa skin tissue in vivo. Mol Ther 2004, 10:318–326
18. Nishie W, Sawamura D, Goto M, Ito K, Shibaki A, McMillan JR, Sakai K, Nakamura H, Olasz E, Yancey KB, Akiyama M, Shimizu H: Humanization of autoantigen. Nat Med 2007, 13:378–383
19. Liu Z, Diaz LA, Troy JL, Taylor AF, Emery DJ, Fairley JA, Giudice GJ: A passive transfer model of the organ-specific autoimmune disease, bullous pemphigoid, using antibodies generated against the hemidesmosomal antigen. BP180 J Clin Invest 1993, 92:2480–2488
20. Engel J, Prockop DJ: The zipper-like folding of collagen triple helices and the effects of mutations that disrupt the zipper. Annu Rev Biophys Biophys Chem 1991, 20:137–152
21. Beck K, Boswell BA, Ridgway CC, Bächinger HP: Triple helix formation of procollagen type I can occur at the rough endoplasmic reticulum membrane. J Biol Chem 1996, 271:21566–21573
22. Söder S, Pöschl E: The NC1 domain of human collagen IV is necessary to initiate triple helix formation. Biochem Biophys Res Commun 2004, 325:276–280
23. Areida SK, Reinhardt DP, Muller PK, Fietzek PP, Kowitz J, Marinkovich MP, Notbohm H: Properties of the collagen type XVII ectodomain: evidence for N- to C-terminal triple helix folding. J Biol Chem 2001, 276:1594–1601
24. Hilal L, Rochat A, Duquesnoy P, Blanchet-Bardon C, Wechsler J, Martin N, Christiano AM, Barrandon Y, Uitto J, Goossens M, Hovnanian A: A homozygous insertion-deletion in the type VII collagen gene (COL7A1) in Hallopeau-Siemens dystrophic epidermolysis bullosa. Nat Genet 1993, 5:287–293
25. Hovnanian A, Rochat A, Bodemer C, Petit E, Rivers CA, Prost C, Fraitag S, Christiano AM, Uitto J, Lathrop M, Barrandon Y, de Prost Y: Characterization of 18 new mutations in COL7A1 in recessive dystrophic epidermolysis bullosa provides evidence for distinct molecular mechanisms underlying defective anchoring fibril formation. Am J Hum Genet 1997, 61:599–610
26. Lejeune F, Maquat LE: Mechanistic links between nonsense-mediated mRNA decay and pre-mRNA splicing in mammalian cells. Curr Opin Cell Biol 2005, 17:309–315
27. Mellerio JE, Dunnill MG, Allison W, Ashton GH, Christiano AM, Uitto J, Eady RA, McGrath JA: Recurrent mutations in the type VII collagen gene (COL7A1) in patients with recessive dystrophic epidermolysis bullosa. J Invest Dermatol 1997, 109:246–249
28. Pulkkinen L, Uitto J: Mutation analysis and molecular genetics of epidermolysis bullosa. Matrix Biol 1999, 18:29–42
29. Gardella R, Castiglia D, Posteraro P, Bernardini S, Zoppi N, Paradisi M, Tadini G, Barlati S, McGrath JA, Zambruno G, Colombi M: Genotype-phenotype correlation in Italian patients with dystrophic epidermolysis bullosa. J Invest Dermatol 2002, 119:1456–1462
30. Kern JS, Kohlhase J, Bruckner-Tuderman L, Has C: Expanding the COL7A1 mutation database: novel and recurrent mutations and unusual genotype-phenotype constellations in 41 patients with dystrophic epidermolysis bullosa. J Invest Dermatol 2006, 126:1006–1012
31. Varki R, Sadowski S, Uitto J, Pfendner E: Epidermolysis bullosa. II. Type VII collagen mutations and phenotype-genotype correlations in the dystrophic subtypes. J Med Genet 2007, 44:181–192

Cell

Genotoxic Stress Abrogates Renewal of Melanocyte Stem Cells by Triggering Their Differentiation

Ken Inomata,[1,2,3] Takahiro Aoto,[1,4] Nguyen Thanh Binh,[1] Natsuko Okamoto,[1,5] Shintaro Tanimura,[1,3] Tomohiko Wakayama,[6] Shoichi Iseki,[6] Eiji Hara,[7] Takuji Masunaga,[2] Hiroshi Shimizu,[3] and Emi K. Nishimura[1,4,*]

[1]Division of Stem Cell Medicine, Center for Cancer and Stem Cell Research, Cancer Research Institute, Kanazawa University, 13-1 Takaramachi, Kanazawa, Ishikawa 920-0934, Japan

[2]Fundamental Research Laboratories, KOSÉ Corporation, 1-18-4 Azusawa, Itabashi-ku, Tokyo 174-0051, Japan

[3]Department of Dermatology, Hokkaido University Graduate School of Medicine, North 15 West 7, Kita-ku, Sapporo 060-8638, Japan

[4]Department of Stem Cell Biology, Medical Research Institute, Tokyo Medical and Dental University, 2-3-10 Kandasurugadai, Chiyoda-ku, Tokyo 101-0062, Japan

[5]Department of Dermatology, Kyoto University Graduate School of Medicine, 54 Shogoin-Kawaharacho, Sakyo-Ku, Kyoto, 606-8507, Japan

[6]Department of Histology and Embryology, Graduate School of Medical Science, Kanazawa University, 13-1 Takara-machi, Kanazawa, Ishikawa 920-0934, Japan

[7]Division of Cancer Biology, The Cancer Institute, Japanese Foundation for Cancer Research, 3-10-6, Ariake, Koto-ku, Tokyo 135-8550, Japan

*Correspondence: nishscm@tmd.ac.jp

DOI 10.1016/j.cell.2009.03.037

SUMMARY

Somatic stem cell depletion due to the accumulation of DNA damage has been implicated in the appearance of aging-related phenotypes. Hair graying, a typical sign of aging in mammals, is caused by the incomplete maintenance of melanocyte stem cells (MSCs) with age. Here, we report that irreparable DNA damage, as caused by ionizing radiation, abrogates renewal of MSCs in mice. Surprisingly, the DNA-damage response triggers MSC differentiation into mature melanocytes in the niche, rather than inducing their apoptosis or senescence. The resulting MSC depletion leads to irreversible hair graying. Furthermore, deficiency of Ataxia-telangiectasia mutated (ATM), a central transducer kinase of the DNA-damage response, sensitizes MSCs to ectopic differentiation, demonstrating that the kinase protects MSCs from their premature differentiation by functioning as a "stemness checkpoint" to maintain the stem cell quality and quantity.

INTRODUCTION

Stem cell systems maintain the homeostasis of tissues, which are constantly subjected to genotoxic stress such as that caused by reactive metabolic byproducts and environmental mutagens. The accumulation of somatic DNA damage is now considered a main cause of the aging process in multicellular organisms (Hasty et al., 2003; Schumacher et al., 2008). Stem cell depletion due to the accumulation of DNA damage has been reported in animals with genomic instability and has been implicated in the decline of tissue renewal capacity and the appearance of aging-related phenotypes (Nijnik et al., 2007; Rossi et al., 2007a; Ruzankina et al., 2007). Stem cell senescence and/or apoptosis are thought to be two major cellular mechanisms for stem cell depletion following DNA damage (Ruzankina et al., 2008; Sharpless and DePinho, 2007). p53 and $p16^{Ink4a}$ are the best characterized regulators of senescence and apoptosis in response to DNA damage, including oncogenic mutations, and have been implicated as "gatekeepers" for tumor suppression as well as in tissue aging (Campisi, 2003a; Lowe et al., 2004; Maier et al., 2004; Sharpless and DePinho, 2007).

Hair graying is one of the most obvious sign of aging. Melanogenesis resulting in hair pigmentation is tightly coupled with the hair regeneration cycle. Hair follicles are constantly renewed by altering phases of growth (anagen), regression (catagen), and rest (telogen) (Figure S1 available online). Hair pigments are produced by differentiated melanocytes in the hair matrix during anagen. Melanocyte maturation is mediated by a lineage differentiation program involving MITF, the master transcriptional regulator for melanocyte development, and its target genes responsible for melanin pigment synthesis (Levy et al., 2006; Vance and Goding, 2004). α-melanocyte-stimulating hormone (MSH) signaling through its receptor melanocortin 1 receptor (MC1R) upregulates MITF to stimulate melanogenesis and eumelanin (black/brown) pigment synthesis (Hearing, 2005; Levy et al., 2006; Yamaguchi et al., 2007). Mature melanocytes required for hair pigmentation are supplied from the melanocyte stem cell (MSC) population. We previously identified immature Dct-lacZ^{+}/KIT^{low} melanoblasts located in the bulge area of hair follicles as MSCs (Nishimura et al., 2002, 2005). The MSC population is maintained in that niche environment throughout the hair cycle and self-renews only at early anagen to provide amplifying and differentiating progenies to the hair matrix for hair pigmentation (Figures 2U and S1) (Nishimura et al., 2002). Furthermore, maintenance of this MSC population becomes incomplete with aging, causing physiological hair graying (Nishimura et al., 2005).

Interestingly, the onset of hair graying is preceded by the appearance of ectopically pigmented melanocytes (EPMs), which have a dendritic morphology, in the niche, suggesting that MSCs are differentiated in the niche (Nishimura et al., 2005). As the stem cell niche is occupied by immature MSCs in non-aged physiological conditions, the appearance of EPMs in the stem cell niche is a distinctive event. However, the cause(s) underlying the aging phenomenon and the possible involvement of the DNA-damage response in the appearance of EPMs have not been studied.

Premature hair graying is seen in progeroid syndromes such as Werner's syndrome and Ataxia-telangiectasia (AT) (Hasty et al., 2003; Martin, 2005) as well as after ionizing radiation (IR) (Cooldige, 1925), which damages DNA and causes DNA double-strand breaks (Ward, 1988). Inactivation of "caretaker genes," including *ATM* (ataxia telangiectasia mutated), a kinase which is a key DNA-damage sensor/transducer, causes genomic instability due to an inefficient DNA-damage response (DDR) and results in progeria that segmentally mimics physiological aging (Kinzler and Vogelstein, 1998; McKinnon, 2004; van Heemst et al., 2007). Indeed, AT patients exhibit premature hair graying (Boder and Sedgwick, 1970; Martin, 2005; Taylor et al., 1975), and ATM deficiency in mice also accelerates IR-induced hair graying (Barlow et al., 1999).

In this study, we examined the impact of DNA damage in quiescent MSCs in vivo and the role of caretaker and gatekeeper genes in the determination of the fate of damaged stem cells as well as the involvement of DNA damage in the hair graying phenotype. Our chronological fate analysis of MSCs revealed that they lose their stem cell immaturity and commit to differentiation in the niche after exposure to excessive genotoxic stress, which results in stem cell depletion and subsequent hair graying. Our results indicate that the MSC system maintains the quality of the stem cell pool by eliminating damaged stem cells via the induction of stem cell differentiation in the niche.

RESULTS

Genotoxic Stress Induces the Ectopic Differentiation of MSCs in the Niche

We explored the effects of IR on the coat color of adult mice. At least 5 Gy of IR on the skin was necessary and sufficient for the stable induction of hair graying (Figures 1A and 1B). Next, to determine whether 5 Gy of IR induces any changes in MSCs preceding the onset of hair graying, we examined the morphological changes of the MSC population using expression of the *Dct-lacZ* transgene that tags the melanocyte lineage or another melanocyte lineage marker, KIT. In control nonirradiated mice, Dct-lacZ$^+$ melanoblasts in the hair follicle bulge, which we previously identified as MSCs (Nishimura et al., 2002), were unpigmented with oval and small cell bodies and coexpressed Kit during anagen (Figures 1C, 1D, and 1F) (Nishimura et al., 2005). In sharp contrast, EPMs with dendritic morphologies, instead of immature melanoblasts, appeared in the bulge area of mid-anagen hair follicles after IR (Figures 1G–1J). Most of the EPMs also expressed Dct-lacZ and KIT (Figures 1H–1J). These changes were followed by the significant loss of differentiated melanocytes in the hair matrix in the following hair cycles and resultant depigmentation of newly grown hair (Figures 1B and 1L).

The appearance of EPMs in the niche and the subsequent hair graying were reproducibly induced by 5 Gy IR and most efficiently when the mice were irradiated at around 7–8 weeks after birth, when most hair follicles on the trunk are well synchronized at the resting stage (telogen). The fact that quiescent MSCs but not their amplifying or differentiated progeny reside in these telogen hair follicles enabled us to selectively chase the fate of MSCs in the niche by irradiating at telogen phase. Synchronous stimulation of hair-cycle progression by the telogen-hair plucking method (Potten, 1970) allowed us to further analyze the chronological changes of MSCs after their synchronized activation at the beginning of the hair growth stage (at 2 days after hair plucking) (Figures 2A–2U and S2C). The activated MSCs self-renew transiently only at anagen II and are maintained in a quiescent (noncycling) state throughout the rest of hair follicle cycle both with or without hair plucking (Nishimura et al., 2002) (Figure S1 and data not shown). IR with hair plucking did not result in any detectable differences from IR without hair plucking regarding the fate of MSCs and the resulting coat color of newly regenerated hair (Figures S3, 1B, and 1G–1J). Furthermore, telogen-hair plucking made it efficient to assess the color of newly grown hair without waiting for the previous hair to fall off. Thus, we took advantage of this chronological analysis method in subsequent experiments to examine the effects of IR on quiescent MSCs and to efficiently trace their fate throughout the hair-cycle progression. As shown in Figure 2, Dct-lacZ$^+$ cells in the bulge (MSCs) of irradiated mice keep their dendritic morphology after their division at anagen II and begin to produce abundant pigments in the cytoplasm along with the hair-cycle progression (Figures 2M, 2N, 2R, and 2S). Those dendritic EPMs in the bulge area of follicles at anagen IV and V mimic exactly the EPMs that we previously found in the MSC niche in aging whisker hair follicles (Nishimura et al., 2005) (Figure 1X). EPMs were induced within the bulge area only after stem cell division but MSCs were kept unpigmented while the follicles remained in telogen even after IR (Figures S3G–S3J and data not shown), suggesting that the preceding stem cell activation at early anagen or stem cell division is necessary for the ectopic pigmentation of MSCs in the niche. Furthermore, all these EPM populations in the niche were negative for CD11b/MAC1, a marker for mature myelomonocytic cells, thus being distinguished from macrophages, and eventually disappeared specifically at anagen VI due to their phagocytosis by surrounding keratinocytes (Figures 2O, 2T, S4, and S5).

To examine the relationship between these changes in MSCs and the color of regenerated hair in subsequent hair cycles, we looked at MSCs in the next hair cycle histologically and the consequent hair pigmentation. MSCs were undetectable in the hair follicle bulge in the following cycle and the hair was unpigmented (Figures 1K–1N). The appearance of EPMs in mid-anagen and the consequent depletion of MSCs in the niche at late anagen led to the depigmentation of newly grown hair (Figures 1K–1O and 1B). Therefore, we conclude that IR abrogates renewal of MSCs by inducing their differentiation in the niche, which causes their depletion and leads to hair depigmentation in subsequent hair cycles.

To test whether pigmentation of MSCs can be commonly induced by other DNA-damage inducers, we treated mice with different genotoxic reagents, including busulfan, mitomycin C,

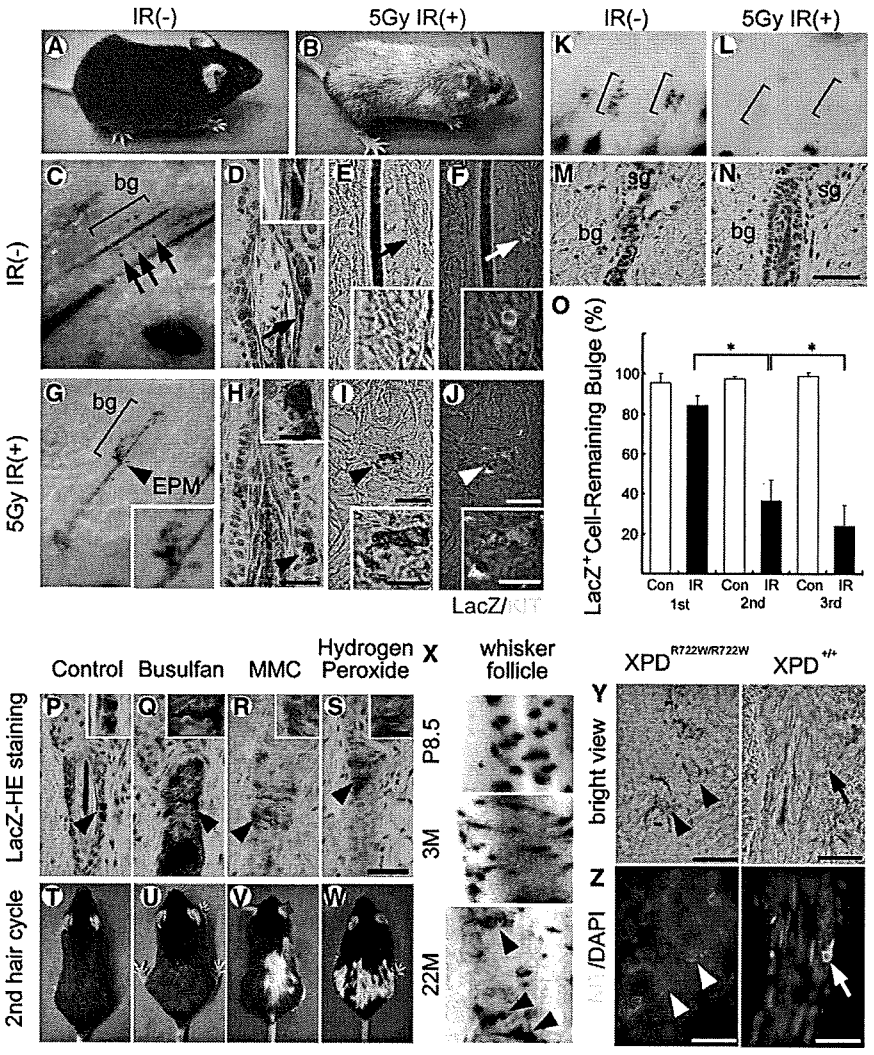

Figure 1. Genotoxic Stress Induces Ectopic Pigmentation of MSCs in the Niche

(A and B) The coat color of control (IR(−)) and X-ray irradiated (5Gy IR(+)) C57BL/6J mice. Hair graying is induced after IR.

(C–J) Histological changes in irradiated hair follicles at anagen V. The bulge areas (bg) of hair follicles on the trunk skin are shown. Whole-mount (C and G) and sectioned lacZ-stained skin from *Dct-lacZ* transgenic mice (D and H). lacZ$^+$ unpigmented melanoblasts (MSCs) were found in the bulge areas of control hair follicles (blue cells with arrows in C and D). (E, F, I, and J) lacZ$^+$ cells (red) in the hair follicle bulge, which coexpress KIT (green), contain no pigment without IR (arrows in E and F) while containing brown-black pigment after IR (arrowheads in I and J) in the bright field view. EPMs with dendritic morphology instead of unpigmented melanoblasts with small and round cell bodies were found in the bulge at 7 days after 5 Gy IR (arrowheads, EPM) (I and J).

(K–N) Disappearance of lacZ$^+$ cells in the hair follicle bulge in the 2nd hair cycle after IR. Whole-mount (K and L) and sectioned lacZ-stained (M and N) skins from control (K and M) and irradiated mice (L and N). Brackets indicate the bulge (bg) areas (K and L).

(O) The frequency of hair follicles that still contain any lacZ$^+$ cells including EPMs in the bulge per total hair follicles in the 1st, 2nd, and 3rd hair cycles after IR.

(P–S) Histological changes in hair follicle bulge areas after treatment with genotoxic reagents. Induction of EPM at 6 days after treatment with busulfan (40 mg/kg body weight) (Q), MMC (Mitomycin C: 4 mg/kg body weight) (R), or hydrogen peroxide (1% in PBS) (S), but not with control vehicle (P). The insets show magnified views of lacZ$^+$ cells indicated by the arrowheads.

(T–W) White hair growth in the 2nd hair cycle after treatment with different genotoxic reagents (U, V, and W) but not with control (T).

(X) Whole-mount lacZ staining of lower permanent portion of whisker hair follicles (stem cell niche) of *Dct-lacZ* transgenic mice at different ages. EPMs with dendritic morphology are found in the niche of aged follicles (22 M, arrowhead).

(Y and Z) The bulge areas of XPD$^{R722W/R722W}$ and XPD$^{+/+}$ 42-week-old mice. KIT$^+$ cells (Z, green) in the hair follicle bulge contain pigment in XPD$^{R722W/R722W}$ mice (arrowheads) but not in control mice (arrows in XPD$^{+/+}$) (Y).

Error bars represent standard error of the mean (SEM); *$p < 0.001$ as calculated by Student's t test. Scale bars represent 25 μm in (H), (I), and (J), 50 μm in (N) and (S), and 10 μm in the insets of (H), (I), (J), and (S). Abbreviations: bg, bulge; sg, sebaceous gland; P, postnatal day; M, month.

and hydrogen peroxide. Local administration of those genotoxic reagents similarly induced EPMs in the bulge and resulted in hair graying in the subsequent hair cycles (Figures 1P–1W). The amount of EPMs in the bulge and the resulting hair depigmentation in subsequent hair cycles varied depending on the chemicals, doses, and skin areas tested (Figures 1U–1W) compared to IR, which induces hair graying and EPMs much more evenly over the entire skin. To further test whether EPMs can be triggered by endogenous DNA damage, we analyzed the hair follicle bulge in XPD$^{R722W/R722W}$ trichothiodystrophy (TTD) mice, which show premature aging phenotypes, such as hair graying (de Boer et al., 2002), that are associated with genetically impaired DNA repair.

EPMs were sporadically found in the bulge area of mid-anagen follicles in XPD$^{R722W/R722W}$ but not in control XPD$^{+/+}$ mice (Figures 1Y and 1Z), suggesting that endogenous DNA damage also triggers the phenomenon. Collectively, these data show that the renewal of MSCs becomes defective with different kinds of genotoxic stress and that the consequent depletion of MSCs causes subsequent hair graying. As the MSC changes and the processes were not distinguishable from the IR-induced EPMs, we further analyzed this phenomenon in *Dct-lacZ* transgenic mice using IR, which induces EPMs and hair graying most efficiently.

DNA-Damage Response in MSCs

To determine whether the DDR is activated in MSCs after IR, we used fluorescent immunohistochemistry to examine foci formation of phosphorylated H2AX (γH2AX), 53BP1, and phosphorylated ATM in hair follicles. We find that DNA-damage foci

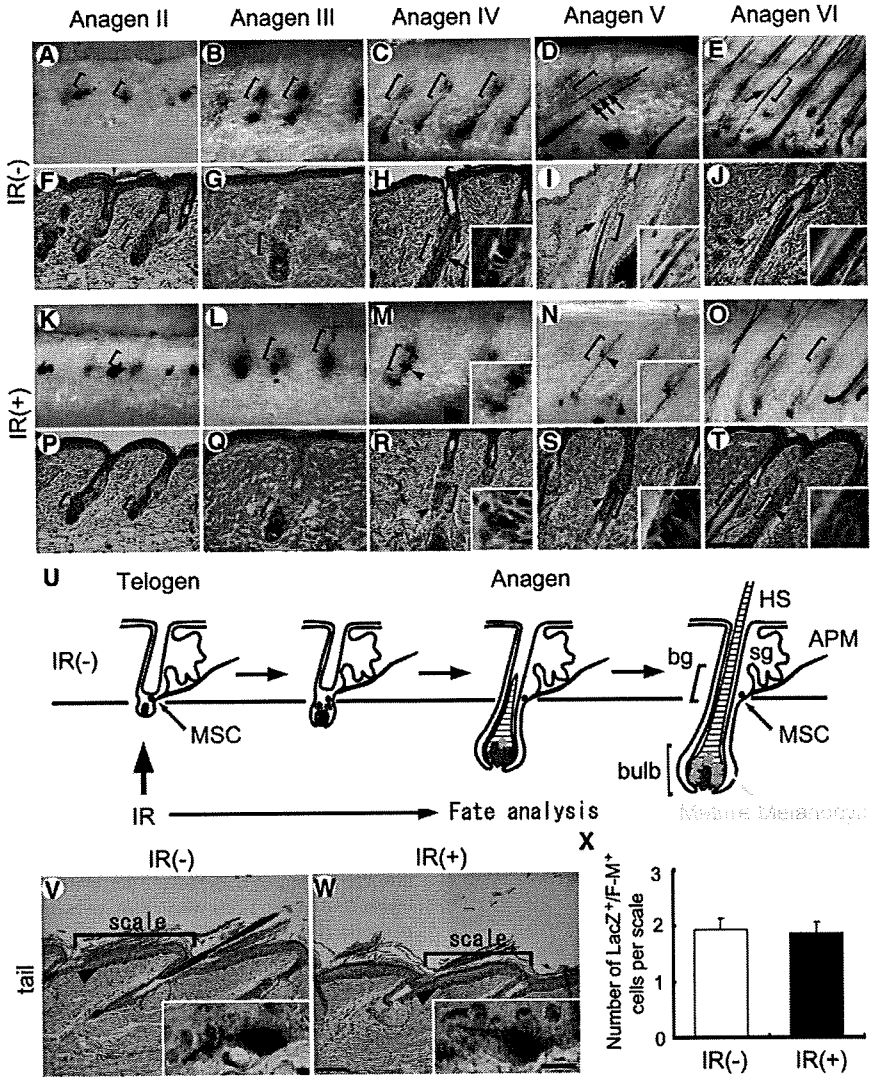

Figure 2. IR Induction of Ectopic Pigmentation and Subsequent Depletion of MSCs in the Niche in Synchronization with Hair-Cycle Progression

Distribution and morphological changes of Dct-lacZ$^+$ cells in irradiated (IR (+)) and control (IR (–)) hair follicles during hair-cycle progression in *Dct-lacZ* transgenic mice. Hair-cycle synchronization was induced by telogen-hair plucking at 7 weeks after birth.

(A–T) Whole-mount (A–E, K–O) and sectioned lacZ-stained skin (F–J, P–T) of *Dct-lacZ* transgenic mice with or without IR. Arrows show lacZ$^+$ cells in bulge area (brackets). EPMs (arrowheads) were observed in the bulge area at anagen IV (M and R) and anagen V (N and S) but disappeared from the bulge area by anagen VI (O and T). Insets show magnified views of lacZ$^+$ cells indicated by the arrows or arrowheads.

(U) A schematic for the MSC fate analysis (shown in A–T) with or without IR at telogen phase.

(V, W, and X) Effects of 5 Gy IR on epidermal melanocytes (lacZ$^+$, blue) in the tail skin of mice that were processed for the above experiments for anagen IV and V follicles. Epidermal melanocytes (lacZ$^+$, blue) in the tail skin are moderately pigmented and did not show any significant changes either in cellular morphology or in pigmentation level with or without IR. The number of lacZ$^+$ Fontana-Masson$^+$ (F-M$^+$) cells per scale (brackets in V and W) are shown in (X). Epidermal melanocytes (V and W) in the hairless skin were refractory to ectopic pigmentation and subsequent disappearance (X). Insets show the magnified views of lacZ$^+$ F-M$^+$ cells indicated by the arrowheads. Scale bars represent 100 μm in (T) and (W) and 10 μm in the insets of (T) and (W). Abbreviations: bg, bulge; sg, sebaceous gland; HS, hair shaft; APM, arrector pili muscle. Error bars in (X) represent SEM.

were induced in the nuclei of cells in hair follicles after IR. Those foci appeared within 3 hr after 5 Gy IR in KIT$^+$ melanoblasts as well as in KIT$^-$ keratinocytes surrounding the bulge area, demonstrating that cells in the bulge area, including MSCs, respond to IR-induced genomic damage (Figure 3). Furthermore, the DNA-damage foci were retained in the nuclei 6 hr after IR followed by a gradual reduction in their number and intensity (Figures 3F, 3H, 3K, and 3L and data not shown). It is notable that some pigmented melanocytes in the niche retain γH2AX foci even at anagen IV (Figures 3K and 3L). These findings suggest that MSCs that incur irreparable levels of IR-induced DNA damage or an excessive DDR have committed to differentiation in the niche.

MSC Commitment to Differentiation Is a Dominant Distinct Fate under Genotoxic Stress

Apoptosis or cellular senescence are two representative cell fates in response to irreparable DNA damage or stress (Campisi, 2003b; Lowe et al., 2004). Our chronological histological analysis showed that Dct-lacZ$^+$ melanocytes are maintained in the bulge area after IR, without showing any histological signs of apoptosis. Indeed, no significant increase of cleaved caspase 3 or TUNEL positivity was found in the skin, including in the bulge area of these follicles, at any time points tested after 5 Gy IR, a dose that is sufficient to induce hair graying (Figures 4A–4C and S6). These data indicate that apoptosis is not likely to be the major early fate of DNA-damaged MSCs.

A senescence-like cellular state in vivo has been demonstrated in human nevi (moles), benign tumors of melanocytes, using senescence-associated β-galactosidase (SA-β-gal) activity and p16^{INK4A} expression as markers (Gray-Schopfer et al., 2006; Michaloglou et al., 2005). We checked SA-β-gal and p16^{INK4A} expression in mouse skin treated with IR to look for signs of a senescence-like phenotype but found neither SA-β-gal nor p16^{INK4A} in the EPMs (Figures 4D–4F, S7B, and S7D). In contrast, a human melanocytic nevus showed SA-β-gal and p16^{INK4A} expression supporting its senescence-like features (Figures 4F, S7E, and S7F), as reported previously (Gray-Schopfer et al., 2006; Michaloglou et al., 2005). These data suggest that neither cellular senescence nor apoptosis is likely to be the major fate of damaged MSCs.

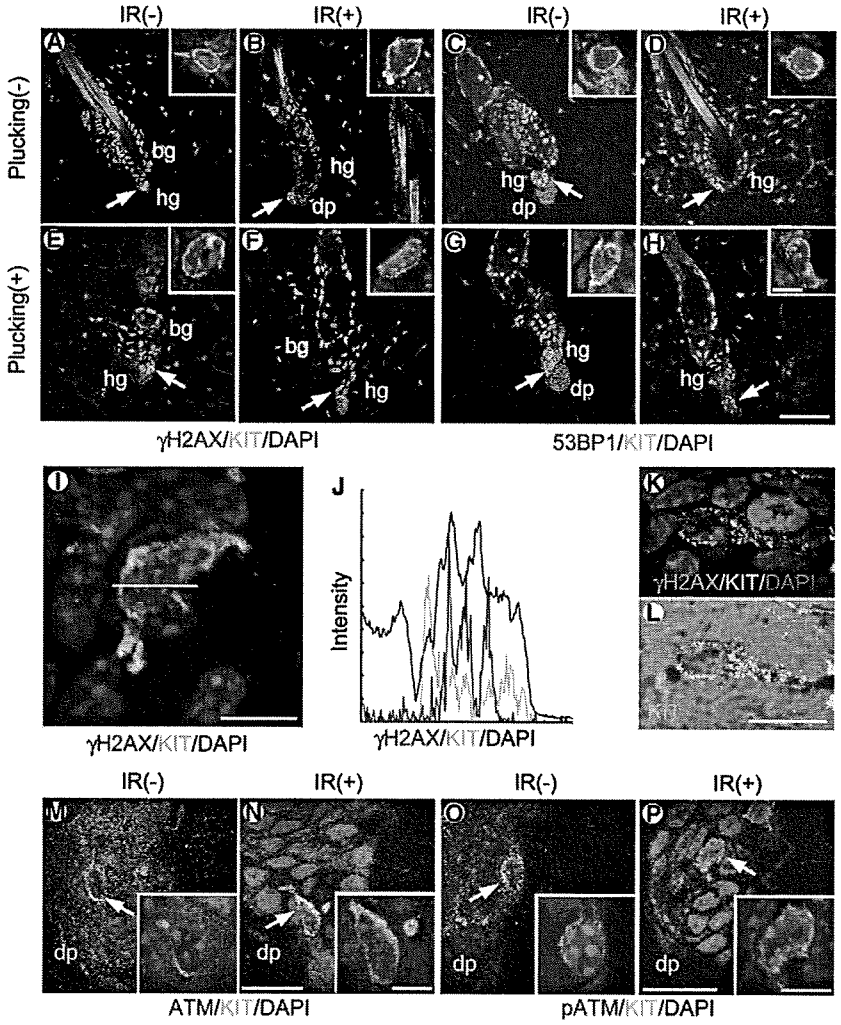

Figure 3. IR Induces DNA-Damage Foci Formation and ATM Activation in the Hair Follicle Bulge

Immunohistochemical analysis for γH2AX, 53BP1, ATM, and p-ATM expression in the hair follicle bulge. Seven-week-old mouse skin, in which almost all hair follicles are synchronized at telogen phase, was irradiated with or without hair plucking and was excised 6 hr after IR.

(A–D) Telogen follicles without IR (control) (A and C) and 6 hr after IR (B and D).

(E–H) Follicles at 1 day after plucking without IR (control) (E and G) and 6 hr after IR (F and H). The distribution of IR-induced DNA-damage foci was indistinguishable in the bulge areas including KIT^+ cells with or without plucking (B, F, D, and H, arrows).

(I) The magnified view of IR-induced γH2AX foci.

(J) Line scan showing fluorescence intensity along the white line overlying the image shown in (I). γH2AX foci (red) were found in the nuclei (blue) of KIT^+ cells (green). Lines were drawn across the nuclei through the foci of KIT^+ cells.

(K and L) IR-induced γH2AX foci remain in KIT^+ EPMs in the bulge area even in mid-anagen follicles (anagen IV). Merged image of the bright field view and KIT immunostaining is shown (L).

(M and N) Expression pattern and subcellular localization of ATM in the hair follicle bulge (arrow). ATM was broadly expressed in the bulge areas including KIT^+ MSCs (arrow) and was mainly localized to the cytoplasm without IR (M). IR induction of ATM localization in the nuclei was found in the bulge cells including KIT^+ cells (arrow) (N).

(O and P) The distribution of p-ATM foci in the bulge area. p-ATM foci were found in the nuclei of bulge cells including KIT^+ cells (arrow) only after IR.

Abbreviations: bg, bulge; dp, dermal papilla; hg, hair germ. Scale bars represent 50 μm in (H), 10 μm in the inset of (H), 10 μm in (I), 5 μm in (L), 15 μm in (N) and (P), and 5 μm in the insets of (N) and (P).

p53 or $p16^{INK4a}$-Rb pathways have been implicated in the fate determination of cells under genotoxic stress including IR (Itahana et al., 2004; Sharpless and DePinho, 2007). To assess the involvement of p53 or $p16^{INK4a}$ pathways in IR induction of EPMs in the niche, we examined expression of p53 and $p16^{INK4a}$ in the bulge after IR. IR induction of p53 expression was transiently detected in Dct-lacZ$^+$ cells in the bulge as well as in the surrounding keratinocytes during early-mid anagen but not at later stages including EPMs (Figures S7H–S7O); $p16^{INK4a}$ expression did not show significant changes with or without IR (Figures S7A–S7D).

We treated *Trp53*$^{-/-}$ and *Ink4a-Arf*$^{-/-}$ mice with IR to test whether p53, $p19^{ARF}$, or $p16^{INK4a}$ are critical for IR induction of EPMs in the niche. EPMs were found in the hair follicle bulge regions in those deficient mice, as seen in wild-type or heterozygous mice (Figures 4H–4K and 4M–4P). Furthermore, the irradiated mutant mice showed hair graying with no significant difference in appearance from their control wild-type and heterozygous mice (Figures 4G and 4L). These findings indicate that p53, $p19^{ARF}$, and $p16^{INK4a}$ are not required for ectopic differentiation of MSCs in the niche and resulting hair graying. These findings also suggest that the IR-induced fate of MSCs is distinct from cellular senescence or apoptosis and is mediated by different signaling pathways.

Genotoxic Stress Triggers the Melanocyte Differentiation Program with Prolonged Activation of Melanocyte Master Regulator MITF in MSCs

As EPMs are mostly dendritic in morphology and are well pigmented, we considered the possibility that genotoxic stress triggers MSC differentiation ectopically through the canonical differentiation program of the melanocyte lineage in the niche. We first examined the expression after IR of the master regulator of the melanocyte lineage, MITF, and downstream melanogenic enzymes, including tyrosinase (TYR) and tyrosinase-related protein 1 (TYRP1), in KIT^+ cells in the bulge area (Figures 5A–5F). In nonirradiated controls, these genes are expressed transiently by MSC progeny in the bulge area after stem cell division at early anagen (anagen II), and their expression becomes downregulated by mid-anagen (anagen IV) (Figures 5A–5C). In contrast, gene expression was prolonged in the stem cell progeny in the bulge areas of IR-radiated follicles

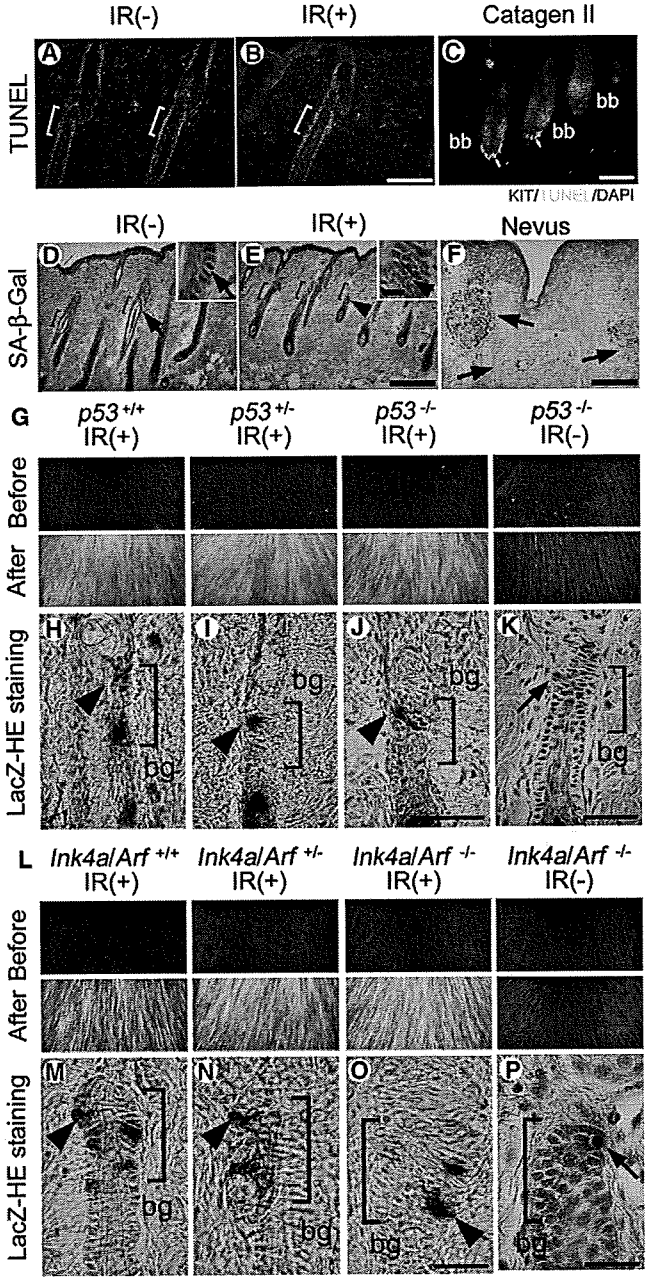

Figure 4. Appearance of EPMs Is Distinct from Apoptotic/Senescence Response and Does Not Require *p53* or *Ink4a/Arf*

(A–C) TUNEL staining of trunk skin from wild-type mice with (B) or without IR (A) and of a catagen II hair follicle as a positive control (C, arrows). TUNEL activity was not found in the hair follicle bulges (brackets) after IR (B). See Figure S6 for more details.

(D–F) Senescence-associated (SA) β-Gal staining of trunk skin from wild-type mice with (E) or without IR (D) and of a human nevus as a positive control (F, arrows). SA-β-Gal activity was not found in EPMs (arrowheads) of hair follicle bulges after IR (E).

(G–P) Effects of IR on MSCs and hair graying in *p53* (G–K) and *Ink4a-Arf*-deficient mice (L–P). (G and L) Changes of coat color before (upper) and after (lower) IR. Hair graying was similarly induced independent of the genetic background of *p53* (G) or *Ink4a/ARF* (L) status. (H–K and M–P) lacZ-stained sections of irradiated (H–J and M–O) or nonirradiated (K and P) hair follicles at anagen IV of various genotypes with *Dct-lacZ* transgene. EPMs were similarly found in the bulge areas in all genotypes (H–J and M–O, arrowheads) after IR. Coat color and MSCs (arrows) in the bulge area of *p53* (K) or *Ink4a/ARF* (P) deficient mice show no overt phenotypes without IR.

The scale bars represent 200 μm in (E) and (F), 10 μm in the inset of (E), 50 μm in (B), (C), (J), and (K), and 25 μm in (O) and (P).

(Figures 5D–5F). These results suggest that MSCs initiate differentiation in the niche via the canonical signaling pathways for melanocyte lineage differentiation.

To test whether the IR induction of melanocyte differentiation is a specific event in activated MSCs in the niche, we examined the differentiation status after IR of epidermal melanocytes located in the basal layer of the epidermis in hairless skin areas such as the tail. We found no differences in the melanin content in lacZ$^+$ epidermal melanocytes with or without 5 Gy IR (Figures 2V–2X). We thus conclude that the induction of EPM is a specific event in activated MSCs at early anagen or is due to their niche microenvironment. As IR induction of melanocyte differentiation was detectable in vitro but less frequently and at lower levels (Figure S8) than seen in activated MSCs, it is likely that the niche microenvironment of early anagen follicles, which usually supports MSC renewal, stimulates the endogenous differentiation program.

Melanosome Formation and Maturation in the Niche

The function of mature melanocytes in the skin is to produce melanin pigments, which are synthesized and polymerized within specialized organelles called melanosomes. Detection of melanosome formation provides reliable functional evidence for melanocyte lineage maturation (Hearing, 2005). To determine whether IR induces melanosome formation in MSCs, first we used transmission electron microscopy (TEM) to establish a method for the ultrastructural analysis of Dct-lacZ$^+$ cells in the bulge area. Dct-lacZ$^+$ cells contained β-galactosidase reaction products deposited on the nuclear membrane (Figures 5G–5J). The cells were small in size and did not contain any melanosomes in the absence of IR treatment (Figure 5I). In contrast, IR treatment induced abundant melanosomes in Dct-lacZ$^+$ cells (EPMs) (Figures 5L and 5N). Melanosome maturation proceeds sequentially in a stepwise manner from stage I to stage IV during the process of melanocyte differentiation and is mediated by MITF target genes (Hearing, 2005). It is notable that typical stage II–III melanosomes (Figure 5N, arrows and arrowhead), which are found only in melanin-synthesizing melanocytes but not in keratinocytes, were present in addition to abundant stage IV melanosomes in EPMs. This finding provides functional evidence of melanocyte maturation with EPMs. Furthermore, the melanosomes in EPMs were indistinguishable from those in physiologically differentiated melanocytes in the hair matrix of mid-anagen hair follicles (Figures 5N and 5O). These findings, in combination with the chronological fate analysis of Dct-lacZ$^+$ cells in the bulge, demonstrate that MSCs in the niche undergo differentiation in response to IR to become pigment-producing dendritic melanocytes through melanosomal maturation.

IR-Induced Melanogenesis Depends on Mc1r but EPM Loss Does Not

The murine recessive yellow allele (Mc1r^e) is a loss-of-function mutation in the MC1R for MSH, which results in yellow hair color

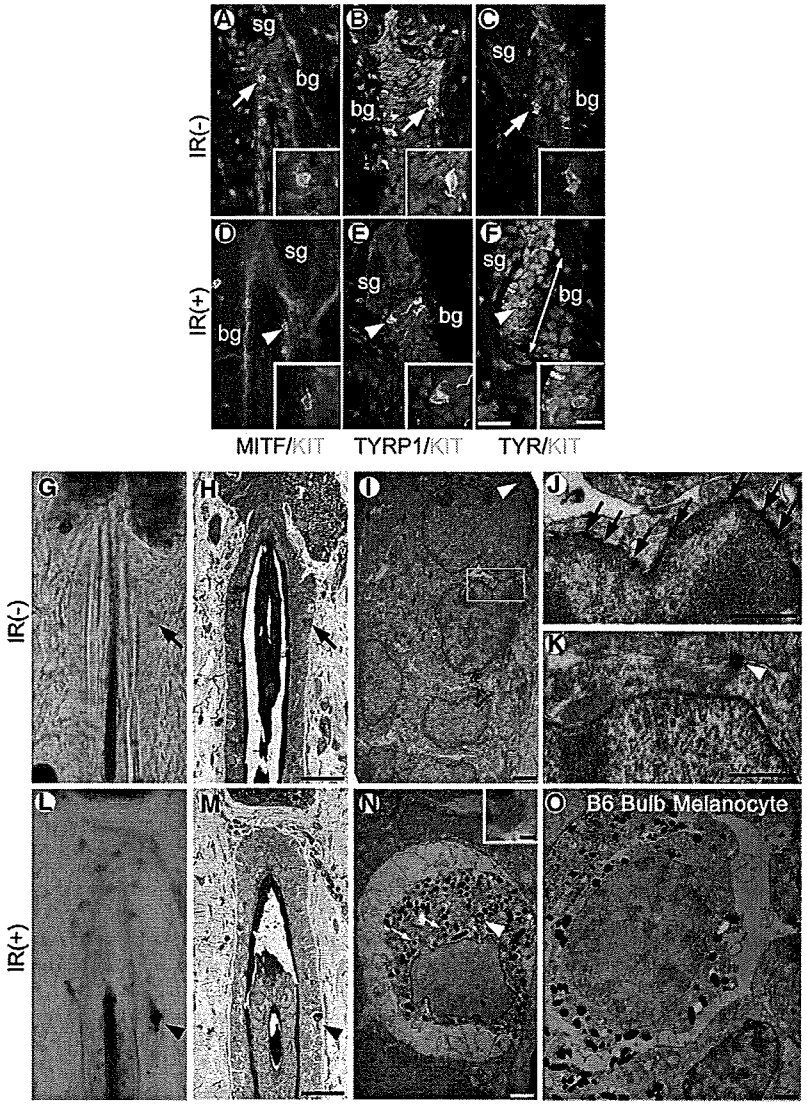

Figure 5. Ectopic Differentiation of MSCs in the Niche with Melanosome Maturation by Activation of the Canonical Differentiation Program

(A–F) Immunohistochemical changes of KIT$^+$ cells in the bulge areas of anagen IV follicles. Expression of MITF (red) and melanogenic enzymes, TYRP1 and TYR (red), is retained in KIT$^+$ cells (green) after IR (D–F, arrowheads) but not in control (A–C, arrows). The insets show magnified views of the KIT$^+$ cells (A–C and D–F).

(G–O) TEM analysis of Dct-lacZ$^+$ cells in the hair follicle bulge areas of *Dct-lacZ* transgenic mice after IR. (G and L) lacZ-stained hair follicles embedded in epoxy resin before sectioning. (H and M) Semi-thin sections with toluidine blue staining of (G) and (L), respectively. (I and N) TEMs of the lacZ$^+$ cells shown in (G) and (L). lacZ$^+$ cells were identified by electron-dense precipitates of X-gal reaction products in the nuclear membrane (I and N, black arrows in J). (J and K) Magnified images of the lacZ$^+$ cells (J) and a lacZ$^-$ keratinocyte (K). A desmosome-like structure (white arrowhead) was found at the cell-cell junction of lacZ$^-$ cells (K). Compared to the control (I), the irradiated lacZ$^+$ EPM contains abundant mature melanosomes (N). The inset in (N) shows a magnified image of a stage II melanosome indicated with the white arrowhead. (O) TEM of a differentiated melanocyte in the bulb of hair follicles of wild-type (C57BL6/J) mice without IR as a positive control. Abbreviations: bg, bulge; sg, sebaceous gland. Scale bars represent 25 μm in (F), (H), and (M), 10 μm in the inset of (F), 1 μm in (I), (N), and (O), 100 nm in the inset of (N), and 500 nm in (J) and (K).

due to pheomelanin (red/yellow pigment) synthesis by hair follicle melanocytes in homozygotes (Figure S9A). Total melanin content and mature melanosome formation are significantly reduced in *Mc1r*$^{e/e}$ melanocytes both in vivo and in vitro (D'Orazio et al., 2006; Hirobe et al., 2007), which indicates that MSH-MC1R signaling promotes melanocyte maturation. To determine whether the IR-induced ectopic differentiation of MSCs and/or the eventual loss of EPMs in the niche depend on MSH-MC1R signaling, extension mutant mice (*Mc1r*$^{e/e}$) and wild-type control mice (*Mc1r*$^{E/E}$) were treated with different doses of IR (Figure S9C–S9L). Melanocytes with dendritic morphology were induced by IR at doses of 5 Gy or 7 Gy but not at less than 3 Gy both in the *Mc1r*$^{E/E}$ controls and in *Mc1r*$^{e/e}$ mice (Figures S9C–S9G). Although IR failed to induce visible pigmentation in MSCs in the absence of functional MC1R, a small number of follicles that contain small amounts of pheomelanin in the bulge of *Mc1r*$^{e/e}$ follicles were clearly detectable (Figures S9M–S9O). These findings indicate that the IR-induced differentiation of MSCs in the niche consists of two steps: a MC1R signaling-independent maturation (as seen in *Mc1r*$^{e/e}$ mutants) and a MC1R signaling-dependent advanced step required for further melanosome maturation and increased melanosome formation. Furthermore, EPMs disappeared from the niche at anagen VI, which resulted in hair graying in subsequent hair cycles in both *Mc1r*$^{e/e}$ and *Mc1r*$^{E/E}$ mice (Figures S9R–S9V, 2N, 2O, 2S, 2T, and S4). These data show that the eventual elimination of EPMs from the niche and the resultant hair graying do not depend on MSH-MC1R signaling or on melanocytic maturation level. This suggests that DDR signaling upstream of MC1R-mediated melanogenic processes determines the eventual fate of damaged stem cells in the niche.

ATM Deficiency Sensitizes MSCs to Ectopic Differentiation in the Niche

By irradiating mice deficient in ATM, we tested whether MSCs undergo differentiation in the niche in response to DNA damage. *Atm*$^{-/-}$ mice showed dramatic hair graying even with 3 Gy IR while *Atm*$^{+/+}$ mice did not gray at all with the same dose of IR (Figure 6A). Consistent with the macroscopic changes, 3 Gy IR induced the appearance of EPMs in the bulge area in *Atm*$^{-/-}$ but not in wild-type controls (Figures 6H–6K). These EPMs induced in *Atm*$^{-/-}$ mice by 3 Gy IR (Figure 6J) were indistinguishable from those induced in wild-type mice by 5 Gy IR (Figures 1 and 2). This indicates that the *Atm* deficiency sensitizes MSCs to differentiate in the niche, resulting in premature hair graying.

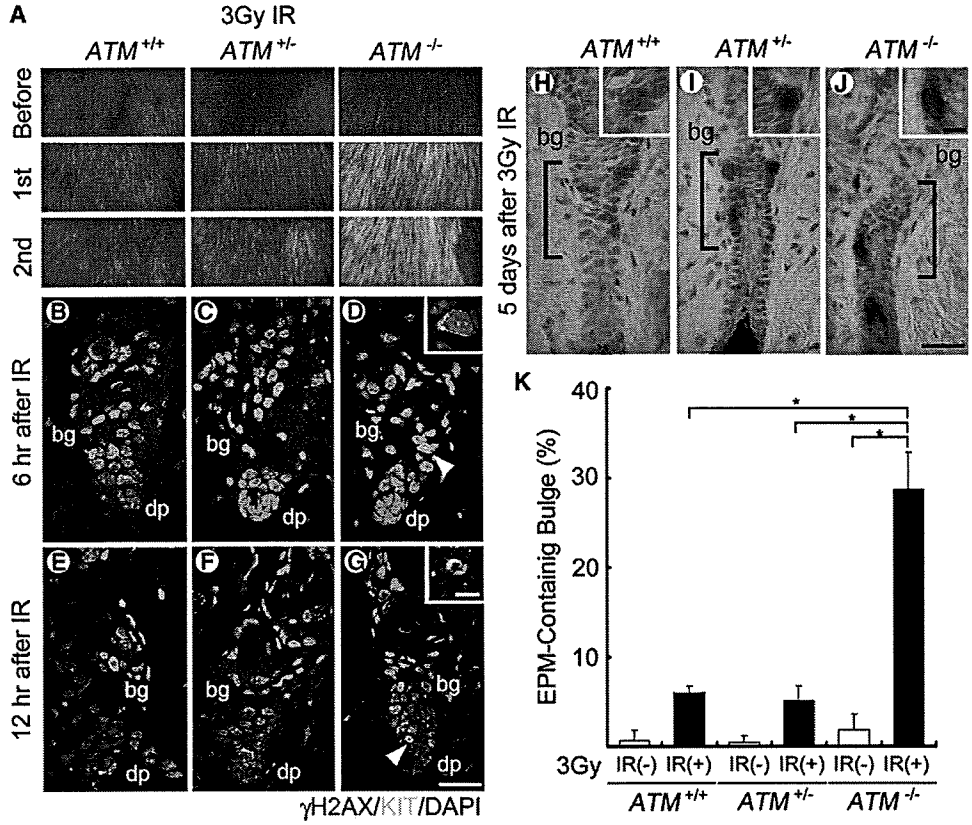

Figure 6. *Atm* Deficiency Sensitizes MSCs to IR-Induced Ectopic Differentiation in the Niche

(A) Changes of coat color in the 1st hair cycle (middle) and the 2nd hair cycle (bottom) after 3 Gy IR compared with before IR (top). Only $Atm^{-/-}$ mice show significant hair graying by 3 Gy IR, a dose normally insufficient to induce hair graying.

(B–G) Immunofluorescent staining of hair follicles for the detection of γH2AX damage foci formation in the bulge area after 3 Gy IR. Foci formation was retained abundantly in $Atm^{-/-}$ follicles including Kit^+ cells even at 12 hr (G). Insets show magnified views of γH2AX foci containing cells indicated with the white arrowheads.

(H–J) Dct-$lacZ^+$ cells in hair follicle bulges from $Atm^{+/+}$ (H), $Atm^{+/-}$ (I), and $Atm^{-/-}$ (J) mice at 5 days after 3 Gy IR. Dendritic EPMs were found in the bulge areas of $Atm^{-/-}$ hair follicles even with 3 Gy IR (J). Insets show magnified views of $lacZ^+$ cells in the bulge areas. The brackets indicate the bulge (bg).

(K) The frequency of hair follicles with EPM in the bulge area per total hair follicles after 3 Gy IR.

Error bars represent SEM; *$p < 0.001$ as calculated by Student's t test. Abbreviations: bg, bulge; dp, dermal papilla. Scale bars represent 25 μm in (G) and (J), 5 μm in the inset of (G), and 10 μm in the inset of (J).

It is notable that DNA-damage foci formation was significantly induced in wild-type mouse skin with 3 Gy IR, a dose which does not induce any detectable changes in coat color and MSC number (Figures 6A and 6H), indicating that ATM efficiently protects MSCs from differentiation at low doses of IR. Furthermore, DNA-damage foci formation in the bulge area after 3 Gy IR was retained significantly longer in *Atm*-deficient mice (Figure 6G), as reported previously for cultured cells (Kuhne et al., 2004; Morrison et al., 2000). This suggests that the DNA-damage repair is inefficient in *Atm*-deficient mice as well as in vitro and that irreparable DNA-damage-induced signals may trigger the differentiation of damaged stem cells at the time of stem cell renewal to maintain the quality of the stem cell pool. Taken together, our data demonstrate that the DDR is involved in the determination of the fate of MSCs, suggesting the existence of a "stemness checkpoint" to maintain the stem cell quality and to prevent hair graying.

DISCUSSION

In Vivo Analysis of the Fate of MSCs under Genotoxic Stress

Stem cells can be characterized by their capacity to self-renew while generating many daughter cells that are committed to differentiation (Fuchs et al., 2004). Stem cell depletion due to the accumulation of DNA damage in the stem cell pool has been implicated in the degradation of tissue renewal capacity and in the appearance of aging-related phenotypes (Nijnik et al., 2007; Rossi et al., 2007a; Ruzankina et al., 2007, 2008). Stem cell exhaustion due to DNA damage has been attributed to apoptosis or senescence of stressed stem cells without detailed stem cell fate-tracing, probably because of technical difficulties (Ruzankina et al., 2008; Simonatto et al., 2007). In this study, we succeeded in analyzing the fate of MSCs under genotoxic stress and found that most MSCs commit to differentiation after stem

cell division. In this system, MSCs and their niche can be visualized and their differentiation status can be assessed by their morphology and most reliably by their pigmentation. The fate of stem cell progeny in the niche can be chronologically analyzed, as the timing of stem cell division can be effectively synchronized by the hair plucking method. MSCs divide at anagen II and the fate of their progeny is determined along with hair-cycle progression by their morphology and pigmentation in addition to lineage markers (Nishimura et al., 2002) (Figures 2 and S1). Furthermore, the functional level of the stem cell system can be assessed by the visible pigmentation of newly grown hair without sacrificing the animals. These advantages allowed us to chronologically analyze the fate of MSCs in hair follicles after exposure to genotoxic stress.

Genotoxic Stress Triggers a Melanocyte Differentiation Program in MSCs

We previously reported that EPMs appear in the stem cell niche prior to aging-related MSC depletion and resultant hair graying (Nishimura et al., 2005). In this study, we found that exposure to multiple genotoxins abrogates renewal of MSCs and induces the commitment of MSC progeny to differentiation in the niche accompanying hair-cycle progression. Our chronological analysis of MSCs revealed that IR induces the prolonged expression of melanogenic genes downstream of MITF and melanosome maturation in MSCs, indicating that MSCs mature into EPMs in the niche in response to IR. Furthermore, our studies with *Mc1r* mutant mice showed that IR-induced melanogenesis in MSC progeny in the niche depends on the *Mc1r*-mediated melanogenesis pathway, which is commonly used for melanocyte maturation and eumelanin pigment synthesis.

While epidermal melanocytes did not respond to IR compared to MSCs in the niche, our in vitro studies showed that IR induced an increased number of differentiated melanocytes in primary culture. Eller et al. also reported that UV and other DNA-damaging reagents can enhance melanogenesis in vitro (Eller et al., 1996). These findings suggest the existence of a cell-autonomous melanogenesis machinery in MSCs as well as the involvement of surrounding niche keratinocytes in the induction of EPMs. Though p53-dependent induction of POMC or KITL/SCF in keratinocytes for paracrine activation of melanocytes has been shown to mediate UV-induced skin tanning or some dark skin phenotypes in mice, respectively (Cui et al., 2007; McGowan et al., 2008), our data showed that the p53 pathway is transiently activated in MSCs after DNA damage but is not required for the induction of EPMs in the niche. Therefore, we conclude that the nodal point for damaged stem cell fate determination is located upstream of *Mc1r*-mediated melanogenic processes and is independent of the p53 pathway or melanocytic maturation level.

Stem Cell Differentiation with Defective Self-Renewal Is a Dominant Fate of Damaged MSCs

Genotoxic stress has been known to trigger cell-cycle arrest to allow DNA repair or induction of apoptosis or senescence in vitro (Campisi, 2003a; van Heemst et al., 2007). Similarly, stem cell senescence or apoptosis have been speculated to be major steps for stem cell depletion due to DNA damage in vivo (Ruzankina et al., 2008). Indeed, this theory is supported by an IR-induced "senescence"-like state characterized by SA-β-gal and p16 expression in purified cells expressing hematopoietic stem cell markers (Meng et al., 2003; Wang et al., 2006). Cell-cycle arrest of muscle progenitor cells under genotoxic stress also has been reported (Puri et al., 2002). However, it is not clear whether it represents a transient cellular response or the eventual fate of the cells and whether the cellular state explains the IR-induced tissue phenotypes.

In the MSC system, we found that stem cell differentiation is the major fate of MSCs under excessive genotoxic stress sufficient for the induction of hair graying. EPMs were induced in the niche within 1 week after IR without showing any significant induction of apoptosis markers or senescence markers. The EPMs are not associated with any morphological characteristics of cultured melanocytes arrested due to replicative senescence, including large, flat, and vacuolated morphology (Bennett and Medrano, 2002; Ha et al., 2008; Medrano et al., 1994). On the other hand, human melanocytic nevi express SA-β-gal and are considered to represent cellular senescence in vivo (Gray-Schopfer et al., 2006; Michaloglou et al., 2005), indicating that EPMs can be distinguished from senescent melanocytes. Though transient induction of p53 expression was found in MSCs after IR, EPMs were found even in *Trp53*-deficient mice and in *Ink4aArf*-deficient mice. Therefore, p53, $p16^{INK4a}$, or $p19^{ARF}$ are not required for the commitment of MSCs to differentiate in the niche in response to DNA damage. Instead, the existence of a stemness checkpoint was demonstrated in this study in mice with inefficient DDR. This new concept is supported by recent in vitro studies with embryonic stem cells, which lose their multipotency and differentiate after DNA damage in vitro (Lin et al., 2005). Therefore, the stemness checkpoint can be rather broadly responsible for DNA-damage-induced stem cell depletion for quality control of the stem cell pool in multiple somatic stem cell systems.

Checkpoint for Renewal of MSCs

Eukaryotic cells respond to DNA damage with a rapid activation of signaling cascades that initiate from the ATR and ATM protein kinases. *ATM* and *ATR* deficiency have been shown to degrade tissue renewal capacity through stem cell depletion with or without exogenous genotoxic stress (Ito et al., 2004; Ruzankina et al., 2007; Takubo et al., 2008). We found that *Atm*-deficient MSCs are sensitized to trigger differentiation in response to DNA damage. As DDR is affected by *Atm* deficiency (Kuhne et al., 2004; McKinnon, 2004; Morrison et al., 2000; Takubo et al., 2008), our data indicate that ATM efficiently protects MSCs from their differentiation in the niche by activating the downstream DDR pathways. Thus, the ATM-mediated DDR is a key for the determination of the fate of MSCs to prevent their premature differentiation and hair graying. Premature hair graying has been reported in *ATR* deficiency in the skin (Ruzankina et al., 2007) and in other repair-deficient progeria model mice, such as $XPD^{R722W/R722W}$ TTD mice (de Boer et al., 2002). As we have detected the significant appearance of EPMs in the bulge area of TTD mice (Figures 1Y and 1Z), stem cell differentiation might be a common general cellular mechanism for stem cell quality control. Therefore, the DNA-damage detection/repair machineries that serve as "caretakers" of the mammalian genome may

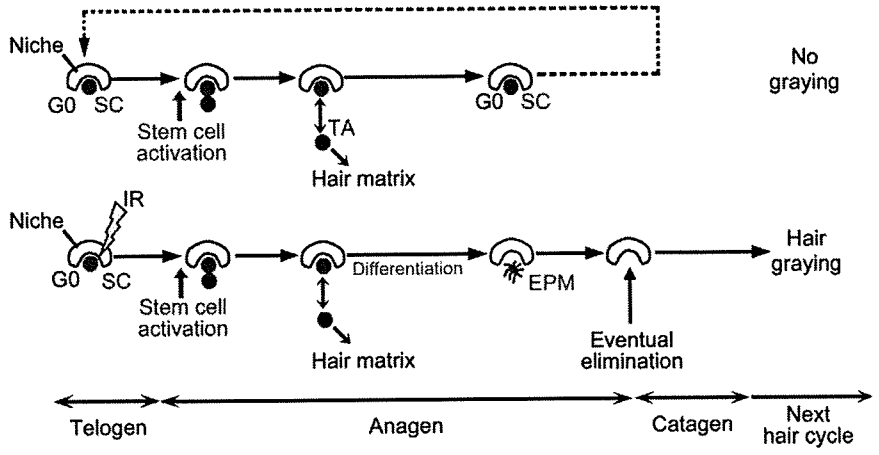

Figure 7. Stem Cell Differentiation Model under Genotoxic Stress

MSCs are maintained in an immature state in the niche throughout hair cycling in nonaged physiological conditions. Transient stem cell activation signals from the niche trigger self-renewal of stem cells at early anagen. The stem cell progeny that remain in the niche re-enter the quiescent state to maintain their stem cell integrity (upper panel). Under irreparable genotoxic stress, such as by IR or chronological aging, MSCs differentiate into EPMs ectopically in the niche without renewing themselves. These EPMs are subsequently eliminated at late anagen. Impaired self-renewal of MSCs through these processes results in hair graying in subsequent hair cycles (lower panel). Abbreviations: SC, stem cells; TA, transit-amplifying cells.

be functioning as a stemness checkpoint in some somatic stem cell systems.

Genotoxic Stress-Induced MSC Differentiation Underlies an Aging-Related Phenotype, Hair Graying

In addition to the aging-associated stem cell depletion typically seen in the MSC system (Nishimura et al., 2005), qualitative and quantitative changes of somatic stem cells have been reported in some stem cell systems, including HSCs, cardiac muscle, and skeletal muscle (Conboy et al., 2003; Morrison et al., 1996; Rossi et al., 2007b; Sussman and Anversa, 2004). Stresses on stem cell pools in genome maintenance failures have also been implicated in the decline of tissue renewal capacity and the accelerated appearance of aging-related phenotypes (Ruzankina et al., 2008). In this study, we discovered that hair graying, the most obvious aging phenotype, can be caused by the genomic damage response through stem cell differentiation, which suggests that physiological hair graying can be triggered by the accumulation of unavoidable DNA damage and DDR associated with aging through MSC differentiation. The EPM found in whisker follicles in aged wild-type mice (Figure 1X) is likely to represent the population. Therefore, our findings support the "stem cell aging hypothesis," which proposes that DNA damage in the long-lived stem cell population can be a major cause for the aging phenotype.

Then, what is the physiological role of stem cell differentiation in response to excessive/irreparable DNA damage? As shown schematically in Figure 7, genotoxic stress-induced EPMs were all eliminated from the niche at late anagen. Removing the damaged/stressed stem cells from the stem cell pool by triggering their differentiation (as the first step) and the eventual elimination of the differentiated damaged cells from the niche (as the second step) may be essential for the quality control of stem cell systems. The stemness checkpoint might be a key protection mechanism of stem cells against cancer development as well as a tissue-aging mechanism.

EXPERIMENTAL PROCEDURES

Animals

Dct-lacZ transgenic mice (a gift from Ian Jackson, MRC) have been described previously (Mackenzie et al., 1997). *XPD* mutant mice (a gift from Jan Hoeijmakers, EMC) (de Boer et al., 2002), *p53*-deficient mice (purchased from Taconic through IBL Japan) (Donehower et al., 1992), *INK4a/ARF*-deficient mice (obtained from the NCI Mouse Models of Human Cancers Consortium [MMHCC]) (Serrano et al., 1996), $MC1R^{e/e}$ mice (obtained from the Jackson Laboratory) (Robbins et al., 1993), and *Atm*-deficient mice (a gift from Peter J. McKinnon, St. Jude Children's Research Hospital) (Herzog et al., 1998) were crossed with *Dct-lacZ* transgenic mice, as described previously (Nishimura et al., 2005). Additional details are provided in the Supplemental Data.

Whole-Body X-Ray Irradiation of Mice

Whole-body X-ray irradiation (IR) was performed using a Hitachi MBR-1520 (Hitachi Medical) operating at 50 kVp, 20 mA with a 2.0 mm Al filter and a dose rate of 0.4 Gy/min. Mice were irradiated at 7–8 weeks old only after confirmation that the skin had a light pink color that indicates that hair follicles are synchronized at the telogen phase. One day after plucking the hair on the dorsal skin, the mice were irradiated (Argyris and Chase, 1960). Irradiation was carried out by placing each mouse in a thin-walled plastic box, after which the animals received whole-body X-rays at dose levels of 1 to 7 Gy. For analysis of the fate of MSCs in the 2nd or 3rd hair cycles, telogen hair depilation was performed with a 30 day interval following the first depilation and the skin was taken 5 days after the last telogen depilation.

Administration of DNA-Damaging Agents

After depilation was performed on the dorsal skin of 7-week-old mice, the mice were subjected to subcutaneous injection of 40 mg/kg body weight Busulfan (Wako Pure Chemicals), 4 mg/kg body weight Mitomycin C (Sigma-Aldrich), or 10 ml/kg body weight 1% hydrogen peroxide (Wako Pure Chemicals).

Immunohistochemical Analysis

Paraffin, frozen sections, and whole-mount β-galactosidase staining were performed as previously described (Nishimura et al., 2002, 2005). Additional details on the methods and antibodies used are provided in the Supplemental Data.

TUNEL Assay

For TUNEL staining (TdT-mediated dUTP-digoxigenin nick end labeling technique), we used the "*in situ* cell death detection kit, Fluorescein" (Roche Diagnostics). Signals were further amplified by Alexa Fluor 488-conjugated anti-fluorescein antibodies (Invitrogen).

Senescence-Associated β-Galactosidase Staining Assay

SA-β-Gal staining was performed on 10 μm-thick cryosections using the "Senescence Cells Histochemical Staining Kit" (Sigma-Aldrich), following the manufacturer's instructions.

Electron Microscopy

Twenty micrometer-thick frozen sections were prepared and stained in X-gal solution at 37°C for 12 hr. For electron microscopy, the sections were post-fixed

in 1% osmium tetroxide for 30 min, stained with 1% uranyl acetate for 20 min, dehydrated in a graded ethanol series, and finally embedded in epoxy resin. Semi-thin sections were stained with toluidine blue and observed by light microscopy. Ultra-thin sections were observed using a transmission electron microscope (JEOL) at 80 kV.

SUPPLEMENTAL DATA

Supplemental Data include Supplemental Experimental Procedures and nine figures and can be found with this article online at http://www.cell.com/supplemental/S0092-8674(09)00374-2.

ACKNOWLEDGMENTS

We thank Dr. Ian Jackson for the *Dct-lacZ* transgenic mice; Dr. Peter McKinnon and Dr. Atsushi Hirao for the *ATM*-deficient mice; Dr. Jan Hoeijmaker for the TTD mice; Dr. Vincent Hearing for antibodies; Dr. Naoko Ohtani, Dr. Kimi Yamakoshi, Dr. Keiyo Takubo, and Dr. Toshio Suda for immunostaining information; Ms. Lica Ishida, Ms. Misa Suzuki, Ms. Yuika Osaki, and Ms. Noriko Ikeda for technical assistance; Mr. Hideki Nakamura for mouse importation; and Dr. Richard Wong and Dr. Hiroyuki Nishimura for critical reading of the manuscript. The research was funded by grants from the Japanese Ministry of Education, Culture, Sports, Science and Technology (17689033, 19390293, 20012017), Uehara Memorial Foundation, and Kato Memorial Bioscience Foundation to E.K.N.

Received: September 9, 2008
Revised: December 15, 2008
Accepted: March 18, 2009
Published: June 11, 2009

REFERENCES

Argyris, T.S., and Chase, H.B. (1960). Effect of x-irradiation on differentating hair follicles. Anat. Rec. *136*, 445–451.

Barlow, C., Eckhaus, M.A., Schaffer, A.A., and Wynshaw Boris, A. (1999). Atm haploinsufficiency results in increased sensitivity to sublethal doses of ionizing radiation in mice. Nat. Genet. *21*, 359–360.

Bennett, D.C., and Medrano, E.E. (2002). Molecular regulation of melanocyte senescence. Pigment Cell Res. *15*, 242–250.

Boder, E., and Sedgwick, R.P. (1970). Ataxia-telangiectasia. (Clinical and immunological aspects). Psychiatr. Neurol. Med. Psychol. Beih. *13–14*, 8–16.

Campisi, J. (2003a). Cancer and ageing: rival demons? Nat. Rev. Cancer *3*, 339–349.

Campisi, J. (2003b). Cellular senescence and apoptosis: how cellular responses might influence aging phenotypes. Exp. Gerontol. *38*, 5–11.

Conboy, I.M., Conboy, M.J., Smythe, G.M., and Rando, T.A. (2003). Notch-mediated restoration of regenerative potential to aged muscle. Science *302*, 1575–1577.

Coolidge, W.D. (1925). High voltage cathode rays outside the generating tube. Science *62*, 441–442.

Cui, R., Widlund, H.R., Feige, E., Lin, J.Y., Wilensky, D.L., Igras, V.E., D'Orazio, J., Fung, C.Y., Schanbacher, C.F., Granter, S.R., et al. (2007). Central role of p53 in the suntan response and pathologic hyperpigmentation. Cell *128*, 853–864.

D'Orazio, J.A., Nobuhisa, T., Cui, R., Arya, M., Spry, M., Wakamatsu, K., Igras, V., Kunisada, T., Granter, S.R., Nishimura, E.K., et al. (2006). Topical drug rescue strategy and skin protection based on the role of Mc1r in UV-induced tanning. Nature *443*, 340–344.

de Boer, J., Andressoo, J.O., de Wit, J., Huijmans, J., Beems, R.B., van Steeg, H., Weeda, G., van der Horst, G.T., van Leeuwen, W., Themmen, A.P., et al. (2002). Premature aging in mice deficient in DNA repair and transcription. Science *296*, 1276–1279.

Donehower, L.A., Harvey, M., Slagle, B.L., McArthur, M.J., Montgomery, C.A., Jr., Butel, J.S., and Bradley, A. (1992). Mice deficient for p53 are developmentally normal but susceptible to spontaneous tumours. Nature *356*, 215–221.

Eller, M.S., Ostrom, K., and Gilchrest, B.A. (1996). DNA damage enhances melanogenesis. Proc. Natl. Acad. Sci. USA *93*, 1087–1092.

Fuchs, E., Tumbar, T., and Guasch, G. (2004). Socializing with the neighbors: stem cells and their niche. Cell *116*, 769–778.

Gray-Schopfer, V.C., Cheong, S.C., Chong, H., Chow, J., Moss, T., Abdel-Malek, Z.A., Marais, R., Wynford-Thomas, D., and Bennett, D.C. (2006). Cellular senescence in naevi and immortalisation in melanoma: a role for p16? Br. J. Cancer *95*, 496–505.

Ha, L., Merlino, G., and Sviderskaya, E.V. (2008). Melanomagenesis: overcoming the barrier of melanocyte senescence. Cell Cycle *7*, 1944–1948.

Hasty, P., Campisi, J., Hoeijmakers, J., van Steeg, H., and Vijg, J. (2003). Aging and genome maintenance: lessons from the mouse? Science *299*, 1355–1359.

Hearing, V.J. (2005). Biogenesis of pigment granules: a sensitive way to regulate melanocyte function. J. Dermatol. Sci. *37*, 3–14.

Herzog, K.H., Chong, M.J., Kapsetaki, M., Morgan, J.I., and McKinnon, P.J. (1998). Requirement for Atm in ionizing radiation-induced cell death in the developing central nervous system. Science *280*, 1089–1091.

Hirobe, T., Abe, H., Wakamatsu, K., Ito, S., Kawa, Y., Soma, Y., and Mizoguchi, M. (2007). Excess tyrosine rescues the reduced activity of proliferation and differentiation of cultured recessive yellow melanocytes derived from neonatal mouse epidermis. Eur. J. Cell Biol. *86*, 315–330.

Itahana, K., Campisi, J., and Dimri, G.P. (2004). Mechanisms of cellular senescence in human and mouse cells. Biogerontology *5*, 1–10.

Ito, K., Hirao, A., Arai, F., Matsuoka, S., Takubo, K., Hamaguchi, I., Nomiyama, K., Hosokawa, K., Sakurada, K., Nakagata, N., et al. (2004). Regulation of oxidative stress by ATM is required for self-renewal of haematopoietic stem cells. Nature *431*, 997–1002.

Kinzler, K.W., and Vogelstein, B. (1998). Landscaping the cancer terrain. Science *280*, 1036–1037.

Kuhne, M., Riballo, E., Rief, N., Rothkamm, K., Jeggo, P.A., and Lobrich, M. (2004). A double-strand break repair defect in ATM-deficient cells contributes to radiosensitivity. Cancer Res. *64*, 500–508.

Levy, C., Khaled, M., and Fisher, D.E. (2006). MITF: master regulator of melanocyte development and melanoma oncogene. Trends Mol. Med. *12*, 406–414.

Lin, T., Chao, C., Saito, S., Mazur, S.J., Murphy, M.E., Appella, E., and Xu, Y. (2005). p53 induces differentiation of mouse embryonic stem cells by suppressing Nanog expression. Nat. Cell Biol. *7*, 165–171.

Lowe, S.W., Cepero, E., and Evan, G. (2004). Intrinsic tumour suppression. Nature *432*, 307–315.

Mackenzie, M.A., Jordan, S.A., Budd, P.S., and Jackson, I.J. (1997). Activation of the receptor tyrosine kinase Kit is required for the proliferation of melanoblasts in the mouse embryo. Dev. Biol. *192*, 99–107.

Maier, B., Gluba, W., Bernier, B., Turner, T., Mohammad, K., Guise, T., Sutherland, A., Thorner, M., and Scrable, H. (2004). Modulation of mammalian life span by the short isoform of p53. Genes Dev. *18*, 306–319.

Martin, G.M. (2005). Genetic modulation of senescent phenotypes in *Homo sapiens*. Cell *120*, 523–532.

McGowan, K.A., Li, J.Z., Park, C.Y., Beaudry, V., Tabor, H.K., Sabnis, A.J., Zhang, W., Fuchs, H., de Angelis, M.H., Myers, R.M., et al. (2008). Ribosomal mutations cause p53-mediated dark skin and pleiotropic effects. Nat. Genet. *40*, 963–970.

McKinnon, P.J. (2004). ATM and ataxia telangiectasia. EMBO Rep. *5*, 772–776.

Medrano, E.E., Yang, F., Boissy, R., Farooqui, J., Shah, V., Matsumoto, K., Nordlund, J.J., and Park, H.Y. (1994). Terminal differentiation and senescence in the human melanocyte: repression of tyrosine-phosphorylation of the extracellular signal-regulated kinase 2 selectively defines the two phenotypes. Mol. Biol. Cell *5*, 497–509.

Meng, A., Wang, Y., Van Zant, G., and Zhou, D. (2003). Ionizing radiation and busulfan induce premature senescence in murine bone marrow hematopoietic cells. Cancer Res. *63*, 5414–5419.

Michaloglou, C., Vredeveld, L.C., Soengas, M.S., Denoyelle, C., Kuilman, T., van der Horst, C.M., Majoor, D.M., Shay, J.W., Mooi, W.J., and Peeper, D.S. (2005). BRAFE600-associated senescence-like cell cycle arrest of human naevi. Nature *436*, 720–724.

Morrison, C., Sonoda, E., Takao, N., Shinohara, A., Yamamoto, K., and Takeda, S. (2000). The controlling role of ATM in homologous recombinational repair of DNA damage. EMBO J. *19*, 463–471.

Morrison, S.J., Wandycz, A.M., Akashi, K., Globerson, A., and Weissman, I.L. (1996). The aging of hematopoietic stem cells. Nat. Med. *2*, 1011–1016.

Nijnik, A., Woodbine, L., Marchetti, C., Dawson, S., Lambe, T., Liu, C., Rodrigues, N.P., Crockford, T.L., Cabuy, E., Vindigni, A., et al. (2007). DNA repair is limiting for haematopoietic stem cells during ageing. Nature *447*, 686–690.

Nishimura, E.K., Jordan, S.A., Oshima, H., Yoshida, H., Osawa, M., Moriyama, M., Jackson, I.J., Barrandon, Y., Miyachi, Y., and Nishikawa, S. (2002). Dominant role of the niche in melanocyte stem-cell fate determination. Nature *416*, 854–860.

Nishimura, E.K., Granter, S.R., and Fisher, D.E. (2005). Mechanisms of hair graying: incomplete melanocyte stem cell maintenance in the niche. Science *307*, 720–724.

Potten, C.S. (1970). Radiation depigmentation of mouse hair: effect of the hair growth cycle on the sensitivity. J. Invest. Dermatol. *55*, 410–418.

Puri, P.L., Bhakta, K., Wood, L.D., Costanzo, A., Zhu, J., and Wang, J.Y. (2002). A myogenic differentiation checkpoint activated by genotoxic stress. Nat. Genet. *32*, 585–593.

Robbins, L.S., Nadeau, J.H., Johnson, K.R., Kelly, M.A., Roselli-Rehfuss, L., Baack, E., Mountjoy, K.G., and Cone, R.D. (1993). Pigmentation phenotypes of variant extension locus alleles result from point mutations that alter MSH receptor function. Cell *72*, 827–834.

Rossi, D.J., Bryder, D., Seita, J., Nussenzweig, A., Hoeijmakers, J., and Weissman, I.L. (2007a). Deficiencies in DNA damage repair limit the function of haematopoietic stem cells with age. Nature *447*, 725–729.

Rossi, D.J., Bryder, D., and Weissman, I.L. (2007b). Hematopoietic stem cell aging: mechanism and consequence. Exp. Gerontol. *42*, 385–390.

Ruzankina, Y., Pinzon-Guzman, C., Asare, A., Ong, T., Pontano, L., Cotsarelis, G., Zediak, V.P., Velez, M., Bhandoola, A., and Brown, E.J. (2007). Deletion of the developmentally essential gene ATR in adult mice leads to age-related phenotypes and stem cell loss. Cell Stem Cell *1*, 113–126.

Ruzankina, Y., Asare, A., and Brown, E.J. (2008). Replicative stress, stem cells and aging. Mech. Ageing Dev. *129*, 460–466.

Schumacher, B., Garinis, G.A., and Hoeijmakers, J.H. (2008). Age to survive: DNA damage and aging. Trends Genet. *24*, 77–85.

Serrano, M., Lee, H., Chin, L., Cordon-Cardo, C., Beach, D., and DePinho, R.A. (1996). Role of the INK4a locus in tumor suppression and cell mortality. Cell *85*, 27–37.

Sharpless, N.E., and DePinho, R.A. (2007). How stem cells age and why this makes us grow old. Nat. Rev. Mol. Cell Biol. *8*, 703–713.

Simonatto, M., Latella, L., and Puri, P.L. (2007). DNA damage and cellular differentiation: more questions than responses. J. Cell. Physiol. *213*, 642–648.

Sussman, M.A., and Anversa, P. (2004). Myocardial aging and senescence: where have the stem cells gone? Annu. Rev. Physiol. *66*, 29–48.

Takubo, K., Ohmura, M., Azuma, M., Nagamatsu, G., Yamada, W., Arai, F., Hirao, A., and Suda, T. (2008). Stem cell defects in ATM-deficient undifferentiated spermatogonia through DNA damage-induced cell-cycle arrest. Cell Stem Cell *2*, 170–182.

Taylor, A.M., Harnden, D.G., Arlett, C.F., Harcourt, S.A., Lehmann, A.R., Stevens, S., and Bridges, B.A. (1975). Ataxia telangiectasia: a human mutation with abnormal radiation sensitivity. Nature *258*, 427–429.

van Heemst, D., den Reijer, P.M., and Westendorp, R.G. (2007). Ageing or cancer: a review on the role of caretakers and gatekeepers. Eur. J. Cancer *43*, 2144–2152.

Vance, K.W., and Goding, C.R. (2004). The transcription network regulating melanocyte development and melanoma. Pigment Cell Res. *17*, 318–325.

Wang, Y., Schulte, B.A., LaRue, A.C., Ogawa, M., and Zhou, D. (2006). Total body irradiation selectively induces murine hematopoietic stem cell senescence. Blood *107*, 358–366.

Ward, J.F. (1988). DNA damage produced by ionizing radiation in mammalian cells: identities, mechanisms of formation, and reparability. Prog. Nucleic Acid Res. Mol. Biol. *35*, 95–125.

Yamaguchi, Y., Brenner, M., and Hearing, V.J. (2007). The regulation of skin pigmentation. J. Biol. Chem. *282*, 27557–27561.